

HIGHER ORDER BEAM THEORIES AND ISOGEOMETRIC METHODS IN THE ANALYSIS OF CURVED BRIDGES - ASSESSMENT OF DIAPHRAGMS' GUIDELINES

Ioannis N. Tsiptsis¹ and Evangelos J. Sapountzakis²

^{1,2}Institute of Structural Analysis and Antiseismic Research, School of Civil Engineering
National Technical University of Athens, Greece
e-mail: mrtsip@hotmail.com, cvsapoun@central.ntua.gr

ABSTRACT: Towards improving conventional beam elements in order to include nonuniform warping effects in the dynamic analysis of bridge decks, in this paper, independent warping parameters have been taken into account and advanced stiffness matrices have been proposed. In addition to this, curved beam's behavior becomes more complex, even for dead loading, due to the coupling between axial force, bending moments and torque that curvature produces. Thus, the importance of simulating geometry exactly arises in order to approximate accurately the response of the curved beam. For this purpose, the Isogeometric tools (b-splines and NURBS), either integrated in the Finite Element Method (FEM) or in a Boundary Element based Method (BEM) called Analog Equation Method (AEM), are employed in this contribution for the static and dynamic analysis of horizontally curved bridge decks of open (I girders) or closed (box-shaped) cross section. Free vibration characteristics and responses of the stress resultants and displacements to static, moving and earthquake loading have been studied. Design guidelines for intermediate diaphragms have been applied for different thin-walled box-shaped bridge decks and assessed as an indirect way to prevent distortional effects.

KEYWORDS: Higher order beam theories (HOBt); curved beam; Nonuniform torsion; Isogeometric Analysis (IGA); spacing of diaphragms;

1. INTRODUCTION

Thin-walled straight or curved structures having open or closed cross-section are widely used in bridge engineering due to their large bending and torsional rigidities as well as their low self-weight. As far as their flexural behavior is concerned, the involved members of these structures are usually analyzed employing beam elements based on Euler-Bernoulli or Timoshenko beam theories. Both of these theories maintain the assumption that cross sections remain plane after deformation. Thus, the formulation remains simple; however

it fails to capture “shear lag” phenomenon, which is associated with a significant modification of normal stress distribution due to nonuniform shear warping [1,2]. This phenomenon has been reported long ago [3-5] in many structural members such as beams of box-shaped cross sections, folded structural members or beams of materials weak in shear. In up-to-date regulations, the significance of shear lag effect in flexure is recognized; however in order to simplify the analysis and permit the use of available conventional finite beam elements, the “effective breadth” concept [6-8] is recommended. This simplifying approach may fail to capture satisfactorily the actual structural behavior of the member, since the influence of shear lag phenomenon is not constant along the beam length, while apart from the geometrical configuration of the cross section it depends also on the type of loading [9,10]. Similar considerations with the ones made for flexure could be also adopted for the torsional problem, which is also very often encountered in the analysis of curved-in-plan bridges. It is well-known, that when a beam undergoes general twisting loading under general boundary conditions, is leaded to nonuniform torsion. This problem has been extensively examined in the literature (e.g. see [11,12]) and its major characteristic is the presence of normal stress due to primary torsional warping. In an analogy with Timoshenko beam theory when shear deformation is of importance, Secondary Torsional Shear Deformation Effect (STSDE) [13,14] has to be taken into account as well. The additional secondary torsional warping due to STSDE causes similar effects with shear lag in flexure, i.e. a modification of the initial normal stress distribution. It is noted that due to the complicated nature of torsion, simplified concepts such as “effective breadth” cannot be applied to take into account this behavior.

The above described effects may become substantial in complex structural forms comprising box-shaped homogeneous or composite cross sections, curved members, short spans or arbitrary loading. Hence a realistic estimation of stress state employing conventional beam elements becomes difficult, since generally commercial programs consider six degrees of freedom (DOFs) at each node of a member of a spatial frame, ignoring in this way all the warping effects due to corresponding warping restraint [15-17]. Therefore, it can be concluded that in order to accurately estimate and assess the actual stress state of a spatial framed structure more rigorous analyses need to be performed.

Even though refined models based on shell or solid finite elements provide the means to perform such analyses, the inclusion of nonuniform warping effects in beam elements based on so-called “Higher-Order Beam Theories” [18,19] is of increased interest due to their important advantages over more elaborate approaches. More specifically

- A Beam formulation reduces significantly modeling effort (solid models require cumbersome post- and pre-processing even in relatively simple

cases).

- It permits isolation of structural phenomena and results interpretation contrary to the reduced oversight of the 3-D FEM models (quantities such as rotation, warping parameter, stress resultants etc. are also evaluated in contrast to solid model which yields only translations and stress components).
- It allows straightforward model handling (support modeling and external loading are easily applied).
- It avoids difficulties in discretizing a complex structure, while the resulting increased number of DOFs of the 3-D models leads to severe or unrealistic computational time.
- It avoids difficulties in discretizing a structure including thin-walled members (shear-, membrane-locking phenomena).
- It facilitates parametric analyses (solid modeling often requires construction of multiple models).
- It does not require shape functions for the kinematical components; hence the minimum number of elements can be employed, while the accuracy of function derivatives is not compromised.
- The use of shell elements cannot give accurate results since warping of the walls of a cross section cannot be taken into account (midline model).

Comparing to straight beam formulations, the behaviour exhibited by curved members is far more complex regarding twist deformations. It is well known, that in case of a horizontally curved beam under transverse loading not only vertical displacement but twist deformation with respect to its longitudinal axis arises as well. Regarding curved beam formulations, a series of straight-line segments is generally used in practice in order to approximate the curved geometry, though ignoring warping transmission between these segments. Vlasov [20] presented a solution for curved beams with open arbitrary cross sections. Then, Dabrowski [21] gave an analysis for closed box-shaped cross sections. Having in mind the above, it is easily concluded that the influence of shear lag phenomenon due to both flexure and torsion, which is not constant along the beam length, should be also considered for curved geometries. The early curved-beam models that have been formulated are either restricted to the analysis of only the beam behaviour in the plane of curvature [22] or do not take into account secondary shear deformation effect caused by nonuniform warping [23, 24], while other efforts consider only doubly symmetric cross sections [25]. In general, even in recent or past years, although the planar problem has been extensively studied, comparatively little work has been done concerning the general three dimensional, non-planar, or coupled lateral-torsional responses of curved beams [22, 25-28]. Regarding the distortional analysis related to the intermediate diaphragms, which is more important for box girders, the number of researches is quite limited. The study related to the distortional analysis of

box girders was initiated by Dabrowski who first formulated the distortional phenomenon of box members with a symmetric cross section [29]. Later and more recently, other research efforts were undertaken regarding the distortional analysis of the structures to give design guidelines on the intermediate diaphragms. Park et al. in [30] and [31] developed a straight and a curved box, respectively, beam finite element having nine degrees of freedom per node in order to propose tentative design charts for adequate maximum spacing of intermediate diaphragms. However, in most of these studies, the placement of diaphragms was not related whether to dynamic property analysis or dynamic response analysis.

When compared to the effort involved in static analysis, there has not been much effort put into the dynamic analysis of curved box girder bridges [32]. The geometric complexities and the spatial coupling effect between bending and torsion make the analysis of curved bridges difficult. Bridge design codes usually provide guidance for the dynamic analysis of straight bridges (dynamic amplification factor, natural frequencies, modelling of vehicles, placement of diaphragms etc.). These design recommendations have been used by some designers for curved bridges, even though some researches carried out [33-35] revealed that need to be reviewed. When bridges are curved, different kinds of loads can cause lateral bending and torsional modes of vibration in addition to the common longitudinal or flexural modes of vibration and so there are still many possible as well as crucial problems to be investigated regarding the dynamic response, for example, forced vibration due to moving loads and earthquake, vehicle-bridge coupling vibration, and wind-induced vibration [36-38]. Some research efforts analyzed out-of-plane vibrations of beams either with uniform or varying cross section and curvature [39,40]. In other studies, the dynamic responses of thin-walled curved box girder bridges due to truck loading have been investigated. The curved box girder bridges has been numerically modelled using finite elements which take into account the torsional warping, distortion and distortional warping [41,42]. However, most of the previous models have been formulated for specific type of loading and cross section either considering or not some higher order phenomena.

In this study, the dynamic generalized warping problem of horizontally curved beams of arbitrary cross section, loading and boundary conditions is presented. This beam element formulated is employed in the analysis of curved bridge decks of open or closed (box-shaped) cross section, taking into account nonuniform warping and shear deformation effects (shear lag due to both flexure and torsion). Except for these effects, curvature influences also the internal forces and deformations of the curved continuous beam, even for dead loading, due to the fact that the curved beam produces coupling between axial force, bending moments and torque, leading to the development of both angle of twist and displacement in the radial direction [45]. The numerical solution of the problem is obtained by Isogeometric tools, either integrated in the Finite

Element Method (FEM) [43] or in a Boundary Element based Method (BEM) called Analog Equation Method (AEM) [44]. To the authors' knowledge Isogeometric analysis is for the first time employed in the design of curved bridges with higher order beam theories, especially combined with a BEM-based method. The developed horizontally curved model takes into account simultaneously in-plane and out-of-plane flexures, extension and torsion and permits the investigation of their coupling. The structure (e.g. bridge deck) is subjected to the combined action of arbitrarily distributed or concentrated axial and transverse loading, as well as to bending, twisting and warping moments. Its edges are subjected to the most general boundary conditions, including also elastic support. Nonuniform warping distributions are taken into account by employing four independent warping parameters multiplying a shear warping function in each direction and two torsional warping functions, which are obtained by solving corresponding boundary value problems, formulated exploiting the longitudinal local equilibrium equation. In this study, the cross section is considered not deformable in its plane through the presence of a sufficient number of diaphragms along the bridge deck, preventing distortion. Design guidelines related to the intermediate diaphragms have been provided to prevent from excessive distortional warping in the longitudinal direction and transverse bending deformation along the cross section perimeter. Thus, fixed values of the stress ratio of the distortional warping normal stress to the bending normal stress are used. Moreover, having in mind that a rigid diaphragm is usually placed in the sections over each pier, both the angle of twist and warping are prevented at these places (bimoment has nonzero values at the support sections). The assessment of these regulations is carried out in this research effort through numerical examples and parametric studies. This could be a natural starting point for the investigation of distortional effects' impact on the analysis of curved bridges. Additional degrees of freedom in order to take into account distortional warping are part of the subsequent research. By employing a distributed mass model system accounting for longitudinal, transverse, rotatory, torsional and warping inertia, ten boundary value problems with respect to the variable along the beam time-dependent 1-D kinematical components are formulated. Free vibration characteristics and responses of the stress resultants and displacements to static, moving and earthquake loading have been studied.

The essential features and novel aspects of the present formulation compared with previous ones are summarized as follows.

- i. The developed beam formulation is capable of the complete analysis (static- [45] and dynamic-present formulation) of spatial curved beams of arbitrary closed or open cross section with one plane of constant curvature (either small or great) considering flexural-torsional shear lag effects and transverse loading to the plane of curvature (as is usually the case in practice). The

necessity to include nonuniform warping and STSD effects in the dynamic analysis of curved bridge decks is demonstrated (for the static analysis refer to [45]).

- ii. The numerical solution of advanced beam theories and its application to the analysis of horizontally curved bridges is based on b-splines [46-47] and NURBS (Isogeometric Analysis) offering the advantage of integrated computer aided design (CAD) in the analysis. Comparing to the previous works of the authors [46-47], where straight beam formulations examined, regarding the use of Isogeometric tools, the present NURBS' formulation allows the integration of the initially curved geometry (which was not previously the case) in the static and dynamic analysis of the advanced beam element employing the same basis functions for the representation of the curve at both deformed and undeformed state. In addition to this, the order of the basis functions is not predefined and can be adjusted by the user.
- iii. The assessment of the design guidelines which specify the maximum spacing of intermediate diaphragms through comparisons of the proposed curved model to the corresponding solid or plate ones and some parametric studies is a first step towards suggesting further provisions and limitations on the application of these regulations.

Numerical examples are worked out to illustrate the method, designate its efficiency, accuracy and computational cost, as well as verify its integrity comparing with the results of traditional methods used for the analysis of bridges. NURBS and b-splines of various degrees have been employed. Knot insertion and degree elevation are proved to be very beneficial in refining the b-spline curve and increasing the accuracy [43]. In addition to this, different radii of curvature have been applied to the model in order to investigate their impact on the arising internal forces.

2. STATEMENT OF THE PROBLEM

2.1 Curved beam model and generalized warping

Let us consider a curved prismatic element of length L with an arbitrarily shaped cross section of homogenous, isotropic and linearly elastic material with modulus of elasticity E and shear modulus G , occupying the region Ω of the yz plane with finite number of inclusions (Fig.1). The cross section can also be

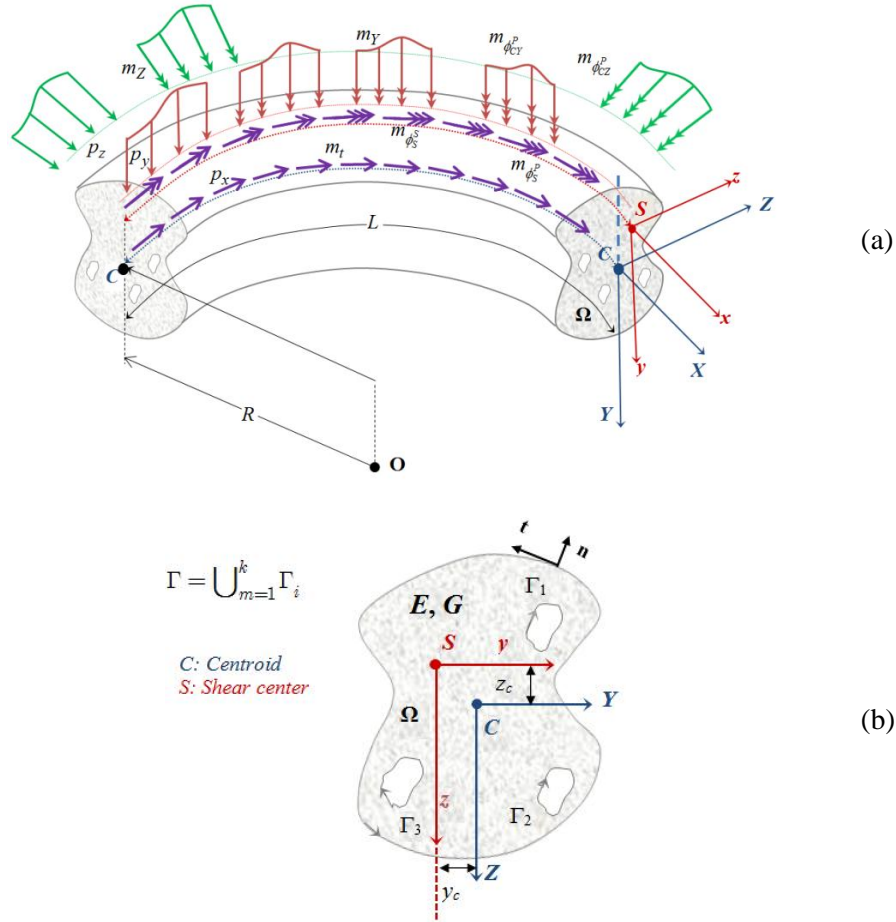


Figure 1. Prismatic curved beam under axial-flexural-torsional loading (a) of an arbitrary homogenous cross section occupying the two dimensional region Ω (b).

considered as composite. Let also the boundary of the region be denoted by. This boundary curve is piecewise smooth, i.e. it may have a finite number of corners. In Fig.1 $CXYZ$ is the principal bending coordinate system through the cross section's centroid C , while y_C, z_C are its coordinates with respect to $Sxyz$ reference coordinate system through the cross section's shear center S . It holds that $y_C = y - Y$ and $z_C = z - Z$. The initial radius of curvature is considered constant, is denoted by R and is parallel to Z axis. The beam element is subjected to the combined action of arbitrarily distributed or concentrated axial loading $p_x = p_x(X)$ along X direction, transverse loading

$p_y = p_y(x)$ and $p_z = p_z(x)$ along the y , z directions, respectively, twisting moments $m_x = m_x(x)$ along x direction, bending moments $m_Y = m_Y(x)$, $m_Z = m_Z(x)$ along Y , Z directions, respectively, as well as to warping moments (bimoments) $m_{\varphi_x^P} = m_{\varphi_x^P}(x)$, $m_{\varphi_Y^P} = m_{\varphi_Y^P}(x)$, $m_{\varphi_Z^P} = m_{\varphi_Z^P}(x)$ and $m_{\varphi_x^S} = m_{\varphi_x^S}(x)$ (Fig.1) [1]. The possible external loading of warping moments is defined in [45].

Under the action of the aforementioned arbitrary external loading and of possible restraints, the beam member is leaded to nonuniform flexure and/or nonuniform torsion. Starting with the flexural behavior of the beam, the following remarks can be made. It is well-known that the bending moment at a beam cross section represents the distribution of normal stresses due to bending (primary normal stresses σ_{xx}^P). Due to the aforementioned bending moment variation along the beam length (nonuniform bending), shear stresses arise on horizontal sections of an infinitesimal curved beam element (Fig.2), equilibrating the variation of normal stresses due to bending. Cauchy principle dictates that corresponding shear stresses arise on the plane of the cross section as well. If the assumption that plane sections remain plane after deformation (Euler-Bernoulli or Timoshenko beam theories) is maintained, the arising shear stresses obtain a uniform distribution over the section [1]. However, this distribution violates local equilibrium since the requirement of vanishing tractions τ_{xn} on the lateral surface of the beam is not satisfied. Thus, the aforementioned shear stresses exhibit a nonuniform distribution over the cross section's domain so that both local equilibrium and vanishing tractions τ_{xn} on the lateral surface of the beam are satisfied. These nonuniform shear stresses will be referred to as primary (or St.Venant) shear stresses (τ_{xy}^P , τ_{xz}^P) and lead the cross section to warp. Furthermore, due to the nonuniform character of this warping along the beam length a secondary normal stress distribution σ_{xx}^S is developed. This normal stress distribution is responsible for the well-known shear lag phenomenon and it is taken into account by employing an independent warping parameter multiplying the warping function, which depends on the cross sectional configuration. The nonuniform distribution of secondary normal stresses σ_{xx}^S along the length of the beam results in the development of secondary shear stresses τ_{xy}^S , τ_{xz}^S , which equilibrate the variation of σ_{xx}^S at an infinitesimal beam element. The above remarks are also valid for the problem of nonuniform torsion taking into account secondary torsional shear deformation

effect – STSDE [1, 13 and 14].

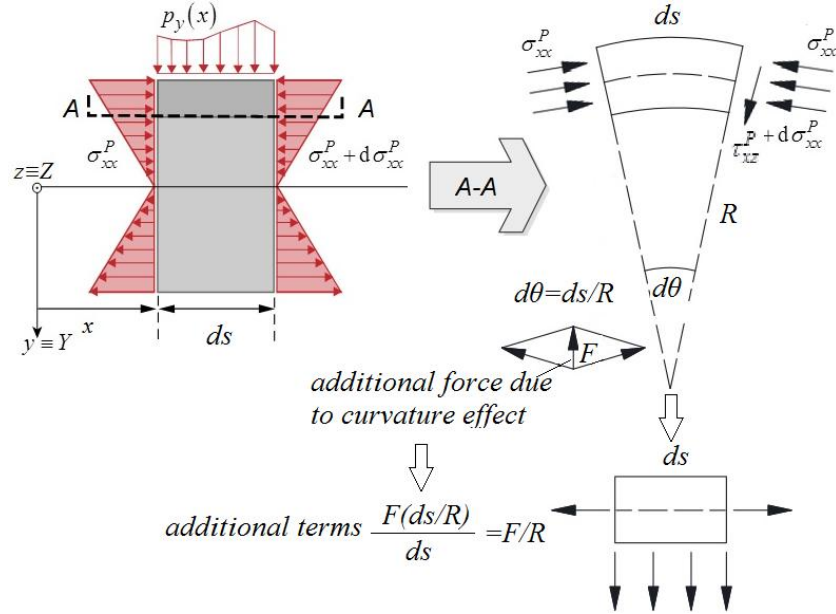


Figure 2. Primary stress of infinitesimal curved beam element and additional terms due to curvature effect. “Perturbed” straight beam formulation.

Within the above described context, in order to take into account nonuniform flexural and torsional warping (including shear lag effect due to both flexure and torsion), in the study of the aforementioned element at each node of the element ends, four additional degrees of freedom are added to the well-known six DOFs of the classical three-dimensional frame element. The additional DOFs include four independent parameters, namely η_x , η_Y , η_Z , ξ_x multiplying a shear warping function in each direction (η_Y , η_Z) and two torsional warping functions (η_x , ξ_x), respectively. These DOFs describe the “intensities” of the corresponding cross sectional warpings along the beam length, while these warpings are defined by the corresponding warping function $(\phi_Y^P, \phi_Z^P, \phi_x^P, \phi_x^S)$, depending only on the cross sectional configuration. Thus, the “actual” deformed configurations of the cross section due to primary (in each direction) shear and primary, secondary torsional warpings are given as $\eta_Y(x,t)\phi_Y^P(y,z)$, $\eta_Z(x,t)\phi_Z^P(y,z)$, $\eta_x(x,t)\phi_x^P(y,z)$ and $\xi_x(x,t)\phi_x^S(y,z)$ at any time instant and position along the beam longitudinal axis, respectively. Moreover, additional terms are added due to curvature effect (Fig. 2) and the

curved beam can be treated as a “perturbed” straight beam avoiding a more refined treatment, which would be more beneficial to geometries with large curvatures. Force F in Fig.2 stands in general for any additional vector (even displacement or strain) that will be added as a result of the differential geometry. Finally, the corresponding stress resultants of the aforementioned additional DOFs are the warping moments $M_{\varphi_Y^P}$, $M_{\varphi_Z^P}$, $M_{\varphi_x^P}$, $M_{\varphi_x^S}$ (bimoments) along the beam length, arising from corresponding normal stress distributions. These bimoments due to the aforementioned warpings constitute additional “higher order” stress resultants, which are developed in the nonuniform shear and torsion theories.

Within the context of the above considerations and for rigid cross section with respect to in-plane deformation, the displacement components of an arbitrary point of the beam at any time instant are given as

$$\begin{aligned} \bar{u}(x, y, z, t) = & \bar{u}^P(x, y, z, t) + \bar{u}^S(x, y, z, t) = \\ & \underbrace{u(x, t) + \theta_Y(x, t)Z - \theta_Z(x, t)Y + \eta_x(x, t)\phi_S^P(y, z)}_{\text{primary}} \\ & + \underbrace{\eta_Y(x, t)\phi_{CY}^P(y, z) + \eta_Z(x, t)\phi_{CZ}^P(y, z) + \xi_x(x, t)\phi_S^S(y, z)}_{\text{secondary}} \end{aligned} \quad (1a)$$

$$\begin{aligned} \bar{v}(x, y, z, t) &= v(x, t) - z\theta_x(x, t) \\ \bar{w}(x, y, z, t) &= w(x, t) + y\theta_x(x, t) \end{aligned} \quad (1b,c)$$

where \bar{u} , \bar{v} , \bar{w} are the axial, transverse and radial beam displacement components with respect to the $Sxyz$ system of axes, while \bar{u}^P , \bar{u}^S , denote the primary and secondary longitudinal displacements, respectively. Moreover, $v(x, t)$, $w(x, t)$ describe the deflection of the centre of twist S , while $u(x, t)$ denotes the “average” axial displacement of the cross section. $\theta_x(x, t)$ is the angle of twist due to torsion, while $\theta_Y(x, t)$, $\theta_Z(x, t)$ are the angles of rotation due to bending about the centroidal Y , Z axes, respectively. $\eta_x(x, t)$, $\xi_x(x, t)$ are the independent warping parameters introduced to describe the nonuniform distribution of primary and secondary torsional warping, while $\eta_Y(x, t)$, $\eta_Z(x, t)$ are the independent warping parameters introduced to describe the nonuniform distribution of primary warping due to shear.

After establishing the displacement field, the strain-displacement relations will be used for the curved beam element described in the previous section. The general shell theory for cylindrical shells [48] can also explain the occurrence of

additional terms. More specifically, the additional terms due to curvature regarding the axial strain ε_{xx} are $\frac{w}{R}$ (which stands for the increase in length due to the radial displacement w according to [49]) and $\frac{\theta_x}{R}$ (which is the decrease in the bending curvature with respect to Z axis). Thus, assuming $\frac{Z}{R} \ll 1$ [28] for the strain in the tangential direction in cylindrical coordinates, the axial strain-displacement relation is given as

$$\varepsilon_{xx} = \left(\bar{u}_{,x} + \frac{w}{R} \right) \cdot \left(1 - \frac{Z}{R} \right) = \left[\underbrace{\left(u_{,x} + \frac{w}{R} + \theta_{Y,x}Z - \left(\theta_{Z,x} - \frac{\theta_x}{R} \right)Y + \eta_{x,x}\phi_S^P \right)}_{\text{primary}} + \underbrace{\left(\eta_{Y,x}\phi_{CY}^P + \eta_{Z,x}\phi_{CZ}^P + \xi_{x,x}\phi_S^S \right)}_{\text{secondary}} \right] \cdot \left(1 - \frac{Z}{R} \right) \quad (2)$$

According to the shear components of strain

$$\begin{aligned} \gamma_{xy} &= (\bar{v}_{,x}) + (\bar{u}_{,y}) = v_{,x} - z\theta_{x,x} + (\bar{u}_{,y}) \\ \gamma_{xz} &= (\bar{w}_{,x}) + (\bar{u}_{,z}) = w_{,x} + y\theta_{x,x} + (\bar{u}_{,z}) \end{aligned} \quad (3a,b)$$

setting as

$$\gamma_x^P = \theta_{x,x} + \frac{\theta_Z}{R} \quad \gamma_Z^P = w_{,x} + \theta_Y - \frac{u}{R} \quad \gamma_Y^P = v_{,x} - \theta_Z \quad (4a,b,c)$$

$$\gamma_x^S = \eta_x - \gamma_x^P = \eta_x - \theta_{x,x} - \frac{\theta_Z}{R}$$

$$\gamma_x^T = \xi_x - \gamma_x^S = \xi_x - \eta_x + \theta_{x,x} + \frac{\theta_Z}{R} \quad (4d,e)$$

$$\gamma_Z^S = \eta_Y - w_{,x} - \theta_Y + \frac{u}{R} \quad \gamma_Y^S = \eta_Z - v_{,x} + \theta_Z \quad (4f,g)$$

and neglecting $\frac{Z}{R}$ effect for shear strains (viewed as higher order term by itself), the shear strain-displacement relations are given as

$$\gamma_{xy} = \underbrace{\left\{ \gamma_Z^P \left[Z_{,y} + \left(\phi_{CY,y}^P \right)_m \right] + \gamma_Y^P \left[Y_{,y} + \left(\phi_{CZ,y}^P \right)_m \right] + \gamma_x^P \left[-z + \left(\phi_{S,y}^P \right)_m \right] \right\}}_{\text{primary}} + \underbrace{\left\{ \gamma_Z^S \left(\phi_{CY,y}^P \right)_m + \gamma_Y^S \left(\phi_{CZ,y}^P \right)_m + \gamma_x^S \left[\left(\phi_{S,y}^P \right)_m + \left(\phi_{S,y}^S \right)_m \right] \right\}}_{\text{secondary}} + \underbrace{\left[\gamma_x^T \left(\phi_{S,y}^S \right)_m \right]}_{\text{tertiary}} \quad (5a)$$

$$\gamma_{xz} = \underbrace{\left\{ \gamma_Z^P \left[Z_{,z} + \left(\phi_{CY,z}^P \right)_m \right] + \gamma_Y^P \left[Y_{,z} + \left(\phi_{CZ,z}^P \right)_m \right] + \gamma_x^P \left[y + \left(\phi_{S,z}^P \right)_m \right] \right\}}_{\text{primary}} + \underbrace{\left\{ \gamma_Z^S \left(\phi_{CY,z}^P \right)_m + \gamma_Y^S \left(\phi_{CZ,z}^P \right)_m + \gamma_x^S \left[\left(\phi_{S,z}^P \right)_m + \left(\phi_{S,z}^S \right)_m \right] \right\}}_{\text{secondary}} + \underbrace{\left[\gamma_x^T \left(\phi_{S,z}^S \right)_m \right]}_{\text{tertiary}} \quad (5b)$$

It is worth here noting that in eqn. (4a), the term $\frac{\theta_Z}{R}$ has been added to the

primary shear strain due to torsion γ_x^P according to the concept presented in Fig. 2. Additionally, the primary transverse shear strain γ_Z^P due to flexure in XZ plane (which is the plane of curvature) is given in eqn. (4b), when employing the equations of general shell theory [48] and considering that the Kirchhoff hypothesis is not valid ($w_{,x} \neq \theta_Y$). On the contrary, the primary transverse shear strain γ_Y^P due to flexure in XY plane is not affected by the curvature and is given in eqn. (4c). The above mentioned expressions of shear strains are also analytically derived according to the refined theory of thick cylindrical shells presented in [50]. Finally, the secondary and tertiary shear strains due to primary and secondary torsional warping of the cross section are given in eqns. (4d,e), respectively, while similarly, the secondary transverse shear strains due to warping in XZ and XY planes of the cross section are given in eqns. (4f,g), respectively.

Employing the Hooke's stress-strain law, the resulting components of the Cauchy stress tensor can be obtained after substituting the components of the strain tensor given in eqns. (2, 5) as $\sigma_{xx} = E\varepsilon_{xx}$, $\tau_{xy} = G\gamma_{xy}$ and $\tau_{xz} = G\gamma_{xz}$. However, as stated above, attention should be paid to the fact that the terms $G\gamma_Z^S \phi_{CY,i}^P$, $G\gamma_Y^S \phi_{CZ,i}^P$, $G\gamma_x^T \phi_{S,i}^S$ ($i = y, z$) are not capable of representing an acceptable shear stress distribution, leading to violation of the longitudinal local equilibrium equation and the corresponding zero-traction condition on the lateral surface of the beam. Thus, a correction of stress components is performed without increasing the number of global kinematical unknowns

according to [1] and [45]. In order to establish the differential equations of equilibrium based on the corrected shear stresses, the principle of virtual work is employed. The geometric constants of the curved beam's cross section are given and explained in [45]. The stress resultants expressed in terms of the kinematical components can be derived according to [1] and [45]. Using the expressions of the strain components (eqns. (2, 5)), the definitions of the stresses and applying the principle of virtual work or any other variational principle following standard arguments in the calculus of variations, the governing differential equations for the curved beam in terms of the kinematical components can be derived. Thus, the local stiffness matrix $[k_t]$ of the spatial curved beam can be evaluated after solving the system of the linear equations. Finally, substituting equations of stress resultants to the differential equations of the curved beam, the equations of equilibrium of the beam are derived as

$$-N_{,x} - \frac{Q_z}{R} = p_x \quad (6a)$$

$$-Q_{y,x} = p_y \quad -Q_{z,x} + \frac{N}{R} = p_z \quad (6b,c)$$

$$-M_{Z,x} - Q_y + \frac{M_t}{R} = m_Z \quad -M_{Y,x} + Q_z = m_Y \quad (6d,e)$$

$$-M_{\phi_{CZ}^P,x} - Q_y^S = m_{\phi_{CZ}^P} \quad -M_{\phi_{CY}^P,x} - Q_z^S = m_{\phi_{CY}^P} \quad (6f,g)$$

$$-M_{t,x} - \frac{M_Z}{R} = m_t \quad (6h)$$

$$-M_{\phi_S^P,x} - M_t^S - M_t^T = m_{\phi_S^P} \quad -M_{\phi_S^S,x} + M_t^T = m_{\phi_S^S} \quad (6i,j)$$

where the externally applied loads are related to the components of the traction vector applied on the lateral surface of the beam t_x, t_y, t_z as

$$p_i(x) = \int_{\Gamma} t_i \, ds, \quad i = x, y, z \quad (7a)$$

$$m_t(x) = \int_{\Gamma} -t_z y + t_y z \, ds \quad (7b)$$

$$m_Y(x) = \int_{\Gamma} t_x Z \, ds \quad m_Z(x) = -\int_{\Gamma} t_x Y \, ds \quad (7c,d)$$

$$m_i(x) = \int_{\Gamma} t_x(i) \, ds, \quad i = \phi_S^P, \phi_{CY}^P, \phi_{CZ}^P, \phi_S^S \quad (7e)$$

The governing differential equations are subjected to the corresponding boundary conditions, which are given as

$$a_1 u + \alpha_2 N_b = \alpha_3 \quad \beta_1 v + \beta_2 V_{by} = \beta_3 \quad \gamma_1 w + \gamma_2 V_{bz} = \gamma_3 \quad (8a,b,c)$$

$$\bar{\beta}_1 \theta_Z + \bar{\beta}_2 M_{bZ} = \bar{\beta}_3 \quad \bar{\gamma}_1 \theta_Y + \bar{\gamma}_2 M_{bY} = \bar{\gamma}_3 \quad (8d,e)$$

$$\tilde{\beta}_1 \eta_Z + \tilde{\beta}_2 M_{b\phi_{CZ}^P} = \tilde{\beta}_3 \quad \tilde{\gamma}_1 \eta_Y + \tilde{\gamma}_2 M_{b\phi_{CY}^P} = \tilde{\gamma}_3 \quad (8f,g)$$

$$\delta_1 \theta_x + \delta_2 M_{bt} = \delta_3 \quad \bar{\delta}_1 \eta_x + \bar{\delta}_2 M_{b\phi_s^P} = \bar{\delta}_3 \quad \tilde{\delta}_1 \xi_x + \tilde{\delta}_2 M_{b\phi_s^S} = \tilde{\delta}_3 \quad (8h,i,j)$$

at the beam ends ($x=0, L$), where the reaction forces N_b , V_{by} , V_{bz} , M_{bZ} , M_{bY} , $M_{b\phi_{CY}^P}$, $M_{b\phi_{CZ}^P}$, M_{bt} , $M_{b\phi_s^P}$, $M_{b\phi_s^S}$ are the stress resultants at the beam ends.

Finally, α_k , β_k , $\bar{\beta}_k$, $\tilde{\beta}_k$, γ_k , $\bar{\gamma}_k$, $\tilde{\gamma}_k$, δ_k , $\bar{\delta}_k$, $\tilde{\delta}_k$ ($k=1,2,3$) are functions specified at the boundaries of the beam ($x=0, L$). The boundary conditions (eqns. (8)) are the most general boundary conditions for the problem at hand, including also the elastic support. It is apparent that all types of the conventional boundary conditions (clamped, simply supported, free or guided edge) can be derived from these equations by specifying appropriately these functions (e.g. for a clamped edge it is

$$\alpha_1 = \beta_1 = \bar{\beta}_1 = \tilde{\beta}_1 = \gamma_1 = \bar{\gamma}_1 = \tilde{\gamma}_1 = \delta_1 = \bar{\delta}_1 = \tilde{\delta}_1 = 1,$$

$$\alpha_2 = \alpha_3 = \beta_2 = \beta_3 = \bar{\beta}_2 = \bar{\beta}_3 =$$

$$\tilde{\beta}_2 = \tilde{\beta}_3 = \gamma_2 = \bar{\gamma}_2 = \tilde{\gamma}_2 = \tilde{\gamma}_3 = \delta_2 = \delta_3 = \bar{\delta}_2 = \bar{\delta}_3 = \tilde{\delta}_2 = \tilde{\delta}_3 = 0).$$

2.2 Curved beams and equations of motion

In order to derive the differential equations of motion with respect to the kinematical components, the terms of inertia contributions $\delta W_{\text{mass}} = \int_V \rho (\bar{u}_{,tt} \delta \bar{u} + \bar{v}_{,tt} \delta \bar{v} + \bar{w}_{,tt} \delta \bar{w}) dV$ have to be added in the previous and constitutive equations should be employed. ρ is the density of the material and $\bar{u}, \bar{v}, \bar{w}$ are the generalized displacements as previously described. Thus, the generalized vibrational beam behaviour is described by the differential equations given in eqns. (9) and the spatial mass matrix $[m_t]$ can finally be derived. Unlike the stiffness matrix and mass matrix of structure, it is not necessary to construct the global damping matrix from the element damping matrix by assembling technique and thus no damping matrix of element is needed to be derived. Much commercial software employs Rayleigh damping which is a linear combination of mass matrix and stiffness matrix. For the proposed curved beam formulation damping is neglected.

$$\begin{aligned} & -EA \left(u_{,xx} + \frac{w_{,x}}{R} \right) - \frac{EI_{YY}}{R} \left(\frac{u_{,xx}}{R} + \frac{w_{,x}}{R^2} - 2\theta_{Y,xx} \right) \\ & - \frac{G}{R} (A_Z^P + A_Z^S) \left(w_{,x} + \theta_Y - \frac{u}{R} \right) + \frac{G}{R} A_Z^S \eta_Y \end{aligned}$$

$$\begin{aligned}
& + \frac{G}{R} \left(D_{\Phi_{CY}^S \Phi_S^S} - D_{\Phi_{CY}^S \Phi_S^T} \right) \left(\eta_x - \theta_{x,x} - \frac{\theta_Z}{R} \right) + \frac{G}{R} D_{\Phi_{CY}^S \Phi_S^T} \xi_x \\
& + \underbrace{\rho A u_{,tt}}_{\text{inertial contribution}} = p_x
\end{aligned} \tag{9a}$$

$$\begin{aligned}
& -G \left(A_Y^P + A_Y^S \right) \left(v_{,xx} - \theta_{Z,x} \right) + G A_Y^S \eta_{Z,x} \\
& + G \left(D_{\Phi_{CZ}^S \Phi_S^S} - D_{\Phi_{CZ}^S \Phi_S^T} \right) \left(\eta_{x,x} - \theta_{x,xx} - \frac{\theta_{Z,x}}{R} \right) + G D_{\Phi_{CZ}^S \Phi_S^T} \xi_{x,x} \\
& + \underbrace{\rho A \left(v_{,tt} - z_C \theta_{x,tt} \right)}_{\text{inertial contribution}} = p_y
\end{aligned} \tag{9b}$$

$$\begin{aligned}
& -G \left(A_Z^P + A_Z^S \right) \left(w_{,xx} + \theta_{Y,x} - \frac{u_{,x}}{R} \right) + G A_Z^S \eta_{Y,x} + G \left(D_{\Phi_{CY}^S \Phi_S^S} - D_{\Phi_{CY}^S \Phi_S^T} \right) \cdot \\
& \cdot \left(\eta_{x,x} - \theta_{x,xx} - \frac{\theta_{Z,x}}{R} \right) + G D_{\Phi_{CY}^S \Phi_S^T} \xi_{x,x} + \frac{EA}{R} \left(u_{,x} + \frac{w}{R} \right) + \\
& + \frac{EI_{YY}}{R^2} \left(\frac{u_{,x}}{R} + \frac{w}{R^2} - 2\theta_{Y,x} \right) + \underbrace{\rho A \left(w_{,tt} + y_C \theta_{x,tt} \right)}_{\text{inertial contribution}} = p_z
\end{aligned} \tag{9c}$$

$$\begin{aligned}
& -EI_{ZZ} \left(\theta_{Z,xx} - \frac{\theta_{x,x}}{R} \right) - G \left(A_Y^P + A_Y^S \right) \left(v_{,x} - \theta_Z \right) + G A_Y^S \eta_Z \\
& + G \left(D_{\Phi_{CZ}^S \Phi_S^S} - D_{\Phi_{CZ}^S \Phi_S^T} \right) \cdot \left(\eta_x - \theta_{x,x} - \frac{\theta_Z}{R} \right) \\
& + G D_{\Phi_{CZ}^S \Phi_S^T} \xi_x - \frac{G}{R} \left(D_{\Phi_{CZ}^S \Phi_S^S} - D_{\Phi_{CZ}^S \Phi_S^T} \right) \left(\eta_Z - v_{,x} + \theta_Z \right) \\
& - \frac{G}{R} \left(D_{\Phi_{CY}^S \Phi_S^S} - D_{\Phi_{CY}^S \Phi_S^T} \right) \cdot \left(\eta_Y - w_{,x} - \theta_Y + \frac{u}{R} \right) \\
& - \frac{G}{R} \left(I_t^S + I_t^T \right) \left(\eta_x - \theta_{x,x} - \frac{\theta_Z}{R} \right) + \\
& + \frac{G}{R} I_t^T \xi_x + \frac{G}{R} I_t^P \left(\theta_{x,x} + \frac{\theta_Z}{R} \right) + \underbrace{\rho I_{ZZ} \theta_{Z,tt}}_{\text{inertial contribution}} = m_Z
\end{aligned} \tag{9d}$$

$$\begin{aligned}
& -EI_{YY}\theta_{Y,xx} + \frac{2EI_{YY}}{R}\left(u_{,xx} + \frac{w_{,x}}{R}\right) + G\left(A_Z^P + A_Z^S\right)\left(w_{,x} + \theta_Y - \frac{u}{R}\right) - GA_Z^S\eta_Y \\
& -G\left(D_{\Phi_{CY}^S\Phi_S^S} - D_{\Phi_{CY}^S\Phi_S^T}\right)\left(\eta_x - \theta_{x,x} - \frac{\theta_Z}{R}\right) - GD_{\Phi_{CY}^S\Phi_S^T}\xi_x \\
& + \underbrace{\rho I_{YY}\theta_{Y,tt}}_{\text{inertial contribution}} = m_Y
\end{aligned} \tag{9e}$$

$$\begin{aligned}
& -E\left(I_{\phi_{CZ}^P\phi_S^P}\eta_{x,xx} + I_{\phi_{CZ}^P\phi_{CY}^P}\eta_{Z,xx} + I_{\phi_{CZ}^P\phi_S^S}\xi_{x,xx}\right) + GA_Y^S\left(\eta_Z - v_{,x} + \theta_Z\right) + \\
& + G\left(D_{\Phi_{CZ}^S\Phi_S^S} - D_{\Phi_{CZ}^S\Phi_S^T}\right)\left(\eta_x - \theta_{x,x} - \frac{\theta_Z}{R}\right) + GD_{\Phi_{CZ}^S\Phi_S^T}\xi_x \\
& + \rho\left(I_{\phi_{CZ}^P\phi_S^P}\eta_{x,tt} + I_{\phi_{CZ}^P\phi_S^S}\xi_{x,tt} + I_{\phi_{CZ}^P\phi_{CY}^P}\eta_{Z,tt}\right) = m_{\phi_{CZ}^P}
\end{aligned} \tag{9f}$$

inertial contribution

$$\begin{aligned}
& -E\left(I_{\phi_{CY}^P\phi_S^P}\eta_{x,xx} + I_{\phi_{CY}^P\phi_{CY}^P}\eta_{Y,xx} + I_{\phi_{CY}^P\phi_S^S}\xi_{x,xx}\right) + GA_Z^S\left(\eta_Y - w_{,x} - \theta_Y + \frac{u}{R}\right) + \\
& + G\left(D_{\Phi_{CY}^S\Phi_S^S} - D_{\Phi_{CY}^S\Phi_S^T}\right)\left(\eta_x - \theta_{x,x} - \frac{\theta_Z}{R}\right) + GD_{\Phi_{CY}^S\Phi_S^T}\xi_x \\
& + \rho\left(I_{\phi_{CY}^P\phi_S^P}\eta_{x,tt} + I_{\phi_{CY}^P\phi_S^S}\xi_{x,tt} + I_{\phi_{CY}^P\phi_{CY}^P}\eta_{Y,tt}\right) = m_{\phi_{CY}^P}
\end{aligned} \tag{9g}$$

inertial contribution

$$\begin{aligned}
& -GI_t^P\left(\theta_{x,xx} + \frac{\theta_{Z,x}}{R}\right) + G\left(I_t^S + I_t^T\right)\left(\eta_{x,x} - \theta_{x,xx} - \frac{\theta_{Z,x}}{R}\right) - GI_t^T\xi_{x,x} + \\
& + G\left(D_{\Phi_{CZ}^S\Phi_S^S} - D_{\Phi_{CZ}^S\Phi_S^T}\right)\left(\eta_{Z,x} - v_{,xx} + \theta_{Z,x}\right) + G\left(D_{\Phi_{CY}^S\Phi_S^S} - D_{\Phi_{CY}^S\Phi_S^T}\right) \cdot \\
& \cdot \left(\eta_{Y,x} - w_{,xx} - \theta_{Y,x} + \frac{u_{,x}}{R}\right) - \frac{E}{R}I_{ZZ}\left(\theta_{Z,x} - \frac{\theta_x}{R}\right) \\
& + \rho\left[A\left(-z_C v_{,tt} + y_C w_{,tt}\right) + I_P\theta_{x,tt}\right] = m_t
\end{aligned} \tag{9h}$$

inertial contribution

$$\begin{aligned}
& -E\left(I_{\phi_S^P\phi_S^P}\eta_{x,xx} + I_{\phi_{CY}^P\phi_S^P}\eta_{Y,xx} + I_{\phi_{CZ}^P\phi_S^P}\eta_{Z,xx}\right) + G\left(I_t^S + I_t^T\right)\left(\eta_x - \theta_{x,x} - \frac{\theta_Z}{R}\right) - \\
& GI_t^T\xi_x + G\left(D_{\Phi_{CZ}^S\Phi_S^S} - D_{\Phi_{CZ}^S\Phi_S^T}\right)\left(\eta_Z - v_{,x} + \theta_Z\right) + G\left(D_{\Phi_{CY}^S\Phi_S^S} - D_{\Phi_{CY}^S\Phi_S^T}\right) \cdot
\end{aligned}$$

$$\cdot \left(\eta_Y - w_{,x} - \theta_Y + \frac{u}{R} \right) + \underbrace{\rho \left(I_{\phi_S^P \phi_S^P} \eta_{x,tt} + I_{\phi_{CY}^P \phi_S^P} \eta_{Y,tt} + I_{\phi_{CZ}^P \phi_S^P} \eta_{Z,tt} \right)}_{\text{inertial contribution}} = m_{\phi_S^P} \quad (9i)$$

$$\begin{aligned} & -E \left(I_{\phi_{CY}^P \phi_S^S} \eta_{Y,xx} + I_{\phi_{CZ}^P \phi_S^S} \eta_{Z,xx} + I_{\phi_S^S \phi_S^S} \xi_{x,xx} \right) + G I_t^T \left(\xi_x - \eta_x + \theta_{x,x} + \frac{\theta_Z}{R} \right) + \\ & + G D_{\Phi_{CZ}^S \Phi_S^T} (\eta_Z - v_{,x} + \theta_Z) + G D_{\Phi_{CY}^S \Phi_S^T} \left(\eta_Y - w_{,x} - \theta_Y + \frac{u}{R} \right) \\ & + \rho \underbrace{\left(I_{\phi_S^S \phi_S^S} \xi_{x,tt} + I_{\phi_{CY}^P \phi_S^S} \eta_{Y,tt} + I_{\phi_{CZ}^P \phi_S^S} \eta_{Z,tt} \right)}_{\text{inertial contribution}} = m_{\phi_S^S} \end{aligned} \quad (9j)$$

The above governing differential equations except for the boundary conditions (eqns. 8) are also subjected to the initial conditions ($x \in (0, L)$)

$$u(x, 0) = u_0(x) \quad u_{,t}(x, 0) = u_{0,t}(x) \quad (10a,b)$$

$$v(x, 0) = v_0(x) \quad v_{,t}(x, 0) = v_{0,t}(x) \quad (10c,d)$$

$$\theta_Z(x, 0) = \theta_{Z0}(x) \quad \theta_{Z,t}(x, 0) = \theta_{Z0,t}(x) \quad (10e,f)$$

$$w(x, 0) = w_0(x) \quad w_{,t}(x, 0) = w_{0,t}(x) \quad (10g,h)$$

$$\theta_Y(x, 0) = \theta_{Y0}(x) \quad \theta_{Y,t}(x, 0) = \theta_{Y0,t}(x) \quad (10i,j)$$

$$\theta_x(x, 0) = \theta_{x0}(x) \quad \theta_{x,t}(x, 0) = \theta_{x0,t}(x) \quad (10k,l)$$

$$\eta_x(x, 0) = \eta_{x0}(x) \quad \eta_{x,t}(x, 0) = \eta_{x0,t}(x) \quad (10m,n)$$

$$\xi_x(x, 0) = \xi_{x0}(x) \quad \xi_{x,t}(x, 0) = \xi_{x0,t}(x) \quad (10o,p)$$

$$\eta_Y(x, 0) = \eta_{Y0}(x) \quad \eta_{Y,t}(x, 0) = \eta_{Y0,t}(x) \quad (10q,r)$$

$$\eta_Z(x, 0) = \eta_{Z0}(x) \quad \eta_{Z,t}(x, 0) = \eta_{Z0,t}(x) \quad (10s,t)$$

After establishing the stiffness and mass matrices of the spatial curved beam element the equation of motion in matrix form can be given as follows

$$[m_t] \{\ddot{U}_i\} + [k_t] \{\bar{U}_i\} = \{p_t\} \quad (11)$$

where $[m_t], [k_t]$ are the generalized mass and stiffness matrices, respectively. $\{p_t\}$ is the load vector which is equal to $\{0\}$ for the free vibration case. $\{\ddot{U}_i\}$ is the vector containing the second derivatives of the different kinematical components with respect to time while $\{\bar{U}_i\}$ is the generalized unknown vector containing the values of the kinematical components and their first derivatives, which will be evaluated numerically.

The natural frequencies and modes in which the beam vibrates for the different motions can be obtained by separation of variables $u_i(x, t)$ which is assumed to have the form

$$u_i(x, t) = u_i(x) e^{i\omega t} \quad (12)$$

where $u_i(x)$ is a function of only the spatial variable x , while $i = \sqrt{-1}$, and ω is the natural frequency. Inserting (12) into (11) and dividing by the common exponential term results in the following typical generalized eigenvalue problem

$$([k_t] - \omega^2 [m_t]) u_i = \{0\} \quad (13)$$

which can be tackled through any solver.

3. NUMERICAL SOLUTIONS FOR CURVED BEAMS

3.1 A BEM-based method combined to isogeometric analysis

The evaluation of the kinematical components $u(x, t)$, $v(x, t)$, $w(x, t)$, $\theta_x(x, t)$, $\theta_Y(x, t)$, $\theta_Z(x, t)$, $\eta_x(x, t)$, $\eta_Y(x, t)$, $\eta_Z(x, t)$ and $\xi_x(x, t)$ is accomplished using the AEM [44]. These have continuous derivatives up to the second order with respect to x at the interval $(0, L)$ and up to the first order at $x = 0, L$ and up to the second order with respect to t , satisfying the initial-boundary value problem described by the coupled governing differential equations of equilibrium (eqns. (9)) along the beam, the initial conditions (eqns. (10)) and the boundary conditions (eqns. (8)) at the beam ends $x = 0, L$.

According to this method, for these functions, the following relation is valid

$$\frac{d^2 u_i(x, t)}{dx^2} = q_i(x, t) \quad (14)$$

where $u_i(x, t)$ are the different kinematical components and $q_i(x, t)$ are the corresponding fictitious loads ($i = 1, \dots, 10$). Eqns. (14) are quasi-static, i.e. the time variable appears as a parameter and they indicate that the solution of eqns. (9), (8), (10) can be established by solving eqns. (14) under the same boundary conditions (eqns. (8)), provided that the fictitious load distributions $q_i(x, t)$ ($i = 1, \dots, 10$) are first established. Isogeometric tools have been employed to approximate both geometry and the fictitious load curve.

The fundamental solution of eqn. (14) is a partial solution of the following differential equation

$$\frac{d^2 u_i^*(x, \xi)}{dx^2} = \delta(x - \xi) \quad (15)$$

where $u_i^*(x, \xi)$ and its derivatives are given as

$$\Lambda_1(x, \xi) = \frac{du_i^*(x, \xi)}{dx} = \frac{1}{2} \operatorname{sgn} r \quad (16a)$$

$$\Lambda_2(x, \xi) = u_i^*(x, \xi) = \frac{1}{2} r \quad (16b)$$

with $r = x - \xi$, x, ξ points of the beam.

Employing this fundamental solution, the integral representation of the kinematical components is obtained as

$$u_i(\xi, t) = \int_0^L \Lambda_2(x, \xi) q_i(x, t) dx - \left[\Lambda_2(x, \xi) \frac{du_i(x, t)}{dx} - \Lambda_1(x, \xi) u_i(x, t) \right]_0^L \quad (17)$$

Eqn. (17) implies that if $q_i(x, t)$ and all boundary values $(u_i(x, t), \frac{du_i(x, t)}{dx})$ at

the beam ends $0, L$ are known, $u_i(x, t)$ can be calculated at any internal point of the beam. Differentiating eqn. (17), the expressions for the derivatives of $u_i(x, t)$ are derived as

$$\frac{du_i(\xi, t)}{d\xi} = - \int_0^L \Lambda_1(x, \xi) q_i(x, t) dx - \left[-\Lambda_1(x, \xi) \frac{du_i(x, t)}{dx} \right]_0^L \quad (18)$$

Then, $q_i(x, t)$ is either approximated with constant elements or quadratic elements [45]. The introduction of b-splines or NURBS in the above mentioned expressions can be done by substituting $q_i(x, t)$ with the polynomial representation of a quadratic b-spline or NURBS with a uniform knot vector Ξ with $\xi \in [0, 1]$, which is the parameter space similar to the classic FE subdivision. The first and last knot values are repeated depending on the b-spline degree p and their multiplicity is usually $p + 1$. In one dimension, basis functions formed are interpolatory at the ends of the parameter space interval (knot vector with multiplicities). However, nonuniform knot vectors and repeated knots can also be used with NURBS. According to [51], the NURBS basis functions can be expressed in terms of b-splines basis defined by the Cox-De Boor recursive formula

$$N_{i,0}(\xi) = \begin{cases} 1 & \text{if } \xi_i \leq \xi < \xi_{i+1} \\ 0 & \text{otherwise} \end{cases}, \quad p = 0 \quad (19a)$$

$$N_{i,p}(\xi) = \frac{\xi - \xi_i}{\xi_{i+p} - \xi_i} N_{i,p-1}(\xi) + \frac{\xi_{i+p+1} - \xi}{\xi_{i+p+1} - \xi_{i+1}} N_{i+1,p-1}(\xi), \quad p \geq 1 \quad (19b)$$

Thus, the basis functions can be derived for the quadratic b-spline as follows.

$$N_{0,2}(\xi) = \frac{\xi-0}{0-0} N_{0,1} + \frac{1-\xi}{1-0} N_{1,1} = \begin{cases} (1-\xi)^2 & \text{if } 0 \leq \xi < 1 \\ 0 & \text{otherwise} \end{cases} \quad (20a)$$

$$N_{1,2}(\xi) = \frac{\xi-0}{1-0} N_{1,1} + \frac{1-\xi}{1-0} N_{2,1} = \begin{cases} 2\xi(1-\xi) & \text{if } 0 \leq \xi < 1 \\ 0 & \text{otherwise} \end{cases} \quad (20b)$$

$$N_{2,2}(\xi) = \frac{\xi-0}{1-0} N_{2,1} + \frac{1-\xi}{1-1} N_{3,1} = \begin{cases} \xi^2 & \text{if } 0 \leq \xi < 1 \\ 0 & \text{otherwise} \end{cases} \quad (20c)$$

The quadratic b-spline curve is defined by

$$C_i(\xi) = \sum_{i=0}^2 N_{i,2}(\xi) P_{ii} \quad (21)$$

where P_{ii} are the control points P_{0i} , P_{1i} and P_{2i} of the initial control polygon shown in Fig. 3. Substituting basis functions to eqn. (21), the expression of the fictitious load $q_i(x, t)$ at any time instant is derived as

$$q_i(x, t) = P_{0i} - 2xP_{0i} + x^2P_{0i} + 2xP_{1i} - 2x^2P_{1i} + x^2P_{2i} \quad (22)$$

Three equidistant collocation points have been used, which are presented in the same figure with the control points (Fig. 3). These points are on the longitudinal axis of the curved beam.

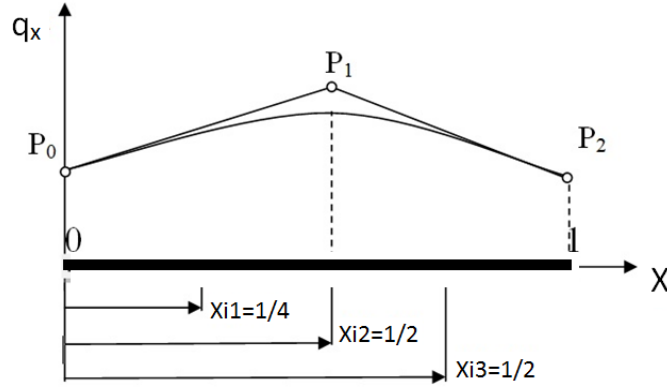


Figure 3. Beam element, representation of fictitious load $q(x, t)$, initial control and collocation points for a kinematical component.

Considering the cubic b-spline, the expression for the fictitious load $q_i(x, t)$ is derived as

$$q_i(x,t) = \frac{(l-x)^3}{l^3} P_{0i} + \frac{3x(l-x)^2}{l^3} P_{1i} + \frac{3x^2(l-x)}{l^3} P_{2i} + \frac{x^3}{l^3} P_{3i} \quad (23)$$

where P_{ii} are the control points P_{0i}, P_{1i}, P_{2i} and P_{3i} .

If four equidistant collocation points for discretization are used, the control polygon of the fictitious load curve and the collocation points are presented in Fig. 4.

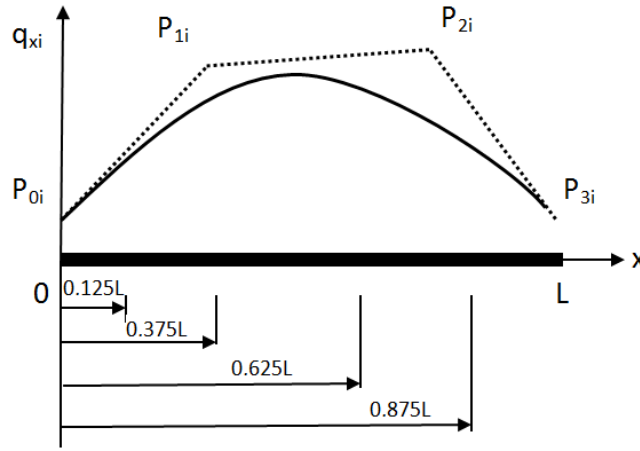


Figure 4. Representation of fictitious load $q(x,t)$ for the cubic b-spline, control and collocation points for a kinematical component (the control polygon is presented in dashed line).

Similarly, the expression for the fictitious load $q_i(x,t)$ for the quartic B-spline is derived as

$$q_i(x,t) = \frac{(L-x)^4}{L^4} P_{0i} + \frac{4x(L-x)^3}{L^4} P_{1i} + \frac{6x^2(L-x)^2}{L^4} P_{2i} + \frac{4x^3(L-x)}{L^4} P_{3i} + \frac{x^4}{L^4} P_{4i} \quad (24)$$

where P_{ii} are the control points $P_{0i}, P_{1i}, P_{2i}, P_{3i}$ and P_{4i} .

Eqns. (17) and (18) written for the boundary points constitute a system of four simultaneous integral equations, while the boundary conditions (8) are formulated in matrix form giving four more equations. Combining the aforementioned equations, the following system is derived

$$\begin{bmatrix} [E_{11}] & [E_{12}] \\ [E_{21}] & [E_{22}] \end{bmatrix} \begin{Bmatrix} \{u_{1i}\} \\ \{u_{2i}\} \end{Bmatrix} = \begin{Bmatrix} \{D_1\} \\ \{0\} \end{Bmatrix} + \begin{Bmatrix} \{0\} \\ \{T_{2i}\} \end{Bmatrix} \rightarrow [E] \{u_i\} = \{D\} + \{T_i\} \quad (25)$$

where $[E]$ is a square 40x40 matrix, $\{u_i\}, \{D\}, \{T_i\}$ are 40x1 vectors, $[E_{11}]$,

$[E_{12}]$ are 20x20 known coefficient matrices and $\{D_1\}$ is 20x1 known coefficient vector, all given in the following equations.

$$[E_{21}]\{u_{1i}\} + [E_{22}]\{u_{2i}\} = \{T_2\} \quad (25a)$$

$$\{T_{2i}\} = - \left\{ \begin{array}{l} \int_0^1 \Lambda_2(x, \xi_0) q_i(x, t) dx \\ \int_0^1 \Lambda_2(x, \xi_1) q_i(x, t) dx \end{array} \right\} \quad (25b)$$

$$\{u_{1i}\}^T = \{u_i'(0) \quad u_i(0)\} \quad (25c)$$

$$\{u_{2i}\}^T = \{u_i'(1) \quad u_i(1)\} \quad (25d)$$

$$[E_{21}] = \begin{bmatrix} \Lambda_2(0, \xi_0) & -(\Lambda_1(0, \xi_0) + 1) \\ \Lambda_2(0, \xi_1) & -\Lambda_1(0, \xi_1) \end{bmatrix} \quad (25e)$$

$$[E_{22}] = \begin{bmatrix} -\Lambda_2(1, \xi_0) & \Lambda_1(1, \xi_0) \\ -\Lambda_2(1, \xi_1) & (\Lambda_1(1, \xi_1) - 1) \end{bmatrix} \quad (25f)$$

$$[E_{11}]\{u_{1i}\} + [E_{12}]\{u_{2i}\} = \{D_1\} \quad (25g)$$

$$\{T_i\} = \begin{bmatrix} [0] \\ \{T_{2i}\} \end{bmatrix} \{P_i\} \rightarrow \{T_i\} = [F]\{P_i\} \quad (25h)$$

Thus, the following system is derived from eqns. (25) and (25h)

$$[E]\{u_i\} = \{D\} + [F]\{P_i\} \rightarrow \{u_i\} = [E]^{-1}\{D\} + [E]^{-1}[F]\{P_i\} \quad (26)$$

With known values at beam ends and applying the integral representations (17) and (18) at the internal collocation points, the following can be calculated

$$\{U_i\} = [A]\{P_i\} + [C]\{u_i\} \quad (27a)$$

$$\{U_i'\} = [A']\{P_i\} + [C']\{u_i\} \quad (27b)$$

where (U_i, U_i') are the vectors containing the values of the different kinematical components and their first derivative at internal collocation points. The coefficients of the square matrices $[A], [A']$ are given by the numerical solution of the integrals in eqns. (28a, b). The $[C], [C'], [C''], [C''']$ matrices are given in eqns. (28c, d).

$$A = \int_{\Gamma_j} \Lambda_2(x, \xi_i) q_i(x, t) dx \quad (28a)$$

$$A' = - \int_{\Gamma_j} \Lambda_1(x, \xi_i) q_i(x, t) dx \quad (28b)$$

$$[C] = \begin{bmatrix} \Lambda_2(0, \xi_1) & -\Lambda_1(0, \xi_1) & -\Lambda_2(l, \xi_1) & \Lambda_1(l, \xi_1) \\ \Lambda_2(0, \xi_2) & -\Lambda_1(0, \xi_2) & -\Lambda_2(l, \xi_2) & \Lambda_1(l, \xi_2) \\ \Lambda_2(0, \xi_3) & -\Lambda_1(0, \xi_3) & -\Lambda_2(l, \xi_3) & \Lambda_1(l, \xi_3) \end{bmatrix} \quad (28c)$$

$$[C'] = \begin{bmatrix} -\Lambda_1(0, \xi_1) & 0 & \Lambda_1(l, \xi_1) & 0 \\ -\Lambda_1(0, \xi_2) & 0 & \Lambda_1(l, \xi_2) & 0 \\ -\Lambda_1(0, \xi_3) & 0 & \Lambda_1(l, \xi_3) & 0 \end{bmatrix} \quad (28d)$$

Substituting eqn. (26) into eqns. (27a, b), the following are derived

$$\{U_i\} = [B]\{P_i\} + \{R\} \quad (29a)$$

$$\{U_i'\} = [B']\{P_i\} + \{R'\} \quad (29b)$$

where

$$[B] = \left[[A] + [C][E]^{-1}[F] \right] \quad (30a)$$

$$[B'] = \left[[A'] + [C'][E]^{-1}[F] \right] \quad (30b)$$

$$\{R\} = [C][E]^{-1}\{D\} \quad (30c)$$

$$\{R'\} = [C'][E]^{-1}\{D\} \quad (30d)$$

Then, the stiffness and mass matrices of the beam element, which behavior is described by eqns. (9) for the dynamic problem, can be calculated employing eqn. (11). Eqns. (9) can be re-written as follows

$$[m_t][B]\{\ddot{q}_t\} + [k_t][\bar{B}]\{q_t\} = \{p_t\} \quad (31)$$

where $\{q_t\}$ in the AEM combined with b-splines or NURBS are the values of the control points while $[\bar{B}]$ contains the coefficients of $[B]$ and $[B']$ matrices. The diagonal matrix $[A_0]$ is also determined and contains the values of basis functions $N_{i,j}$ ($i = 1 \dots n$ and $j = 2 \dots p$) for the n different collocation points and different p -degree b-spline cases. Then, $[m_t]$, $[k_t]$ are formulated and eqn. (31) is solved.

Instead of b-splines, NURBS curves in terms of b-spline basis functions can be employed in the AEM technique. Their expressions are given in the following section.

3.2 FEM and NURBS numerical solutions

The problem described in section 2.1 can be set in the equivalent variational formulation through the principal of virtual work and finally derive eqns (9). In order to discretize eqns. (9), the displacement field $u_i(x)$ given in section 3.1 is approximated by means of polynomial interpolating functions of p -degree as extensively is described in [52]. Substituting the displacement approximation for each discretization element (n in total), the equilibrium equations in terms of the nodal displacements of the finite element mesh can be expressed. Thus, $[k_t]$ matrix can be obtained by assembling the contributions from the individual elements. This can be performed numerically by using the Gauss quadrature rule. In order to compute Gauss base points and weight factors an algorithm has been employed according to [53]. The same procedure can be followed in the AEM technique, with quadrature nodes being the collocation points, if the analytical solution of the integrals employed needs to be avoided for computational reasons. The assembling of “stiffness” matrix $[\bar{B}]$ is different in this case, too.

As a next step in discretizing eqns. (9), p -degree NURBS interpolating functions can be employed for the representation of the displacement field $u_i(x)$. In this case, curve C given in eqn. (21) has a p -degree NURBS representation defined by

$$C_i(\xi) = \sum_{i=1}^n R_{i,p}(\xi) P_{ii} \quad (32)$$

where P_{ii} are the control points employed for each kinematical component and $R_{i,p}(\xi)$, which are the NURBS basis functions, can be expressed as follows

$$R_{i,p}(\xi) = \frac{N_{i,p}(\xi) w_i}{\sum_{i=1}^n N_{i,p}(\xi) w_i} \quad (33)$$

where $N_{i,p}(\xi)$ are given in eqns. (19) and w_i ($\in \mathbb{R}$) are weights related to the i th control point and increase the capabilities of the b-splines interpolation ([43]). Values of the basis functions and their derivatives will be obtained for each quadrature node. It should be noted that if all weights are equal, then $R_{i,p}(\xi) = N_{i,p}(\xi)$ and curve C is a b-spline curve. In addition to this, the geometry of the beam is described by a NURBS structure through an initial control polygon given by the following spatial coordinates (x_i, y_i, z_i, w_i) . This polygon will be later refined as new knots will be inserted and degree will be

elevated in order to achieve more accurate results. $[k_t]$ matrix can finally be obtained following the same procedure as previously described for the AEM technique.

Non-uniform knot vectors Ξ and repeated knots are the key ingredients of NURBS flexibility. In addition to this, among all the properties of NURBS interpolation the most interesting is the high degree of continuity ([43]).

4. NUMERICAL EXAMPLES - ASSESSMENT OF DIAPHRAGMS' GUIDELINES

In order to validate the proposed formulation of the curved beam element described above and examine the advantages attained by the use of the methods proposed in terms of simplicity, accuracy and computational effort, computer programs have been written and representative examples have been studied. The numerical results have been obtained employing NURBS, beam FEs and constant or quadratic elements for the representation of the AEM fictitious loads. Then, the results are compared to those obtained by the application of the Finite Element Method (FEM) employing beam, solid (quadrilateral or triangular) or plate elements. The computer software FEMAP 2008 [54] has been used for this purpose. In addition to these, up to 400 boundary elements depending on the cross section type (cross sectional discretization) have been employed in order to evaluate the geometric constants with BEM.

As another part of this section, design guidelines for specifying the maximum spacing of intermediate diaphragms have been applied to the aforementioned solid models and compared to the proposed one which does not take into account distortional effects. Three different examples of box-shaped cross sections subjected to different geometric limits have been examined. According to thin-walled theory, the upper bounds of these limit sets are $t/d < 0.1$ and $d/L < 0.1$, where t , d and L are the thickness, width and length of the curved box-shaped cross section, respectively.

4.1 Extremely thin-walled monosymmetric box-shaped cross section ($t/d = 0.02, d/L = 0.1$)

In this example, in order to investigate the importance of warping in the analysis of beams as proposed in this study as well as the placement of intermediate diaphragms, the static problem of a monosymmetric box shaped straight cantilever bridge beam during its erection phase is examined. Its cross section is shown in Fig. 5 ($E = 4 \times 10^7 \text{ kN/m}^2$, $G = 2 \times 10^7 \text{ kN/m}^2$ - these properties have been selected for comparison reasons and give $\nu = 0$, $\rho = 7.85 \text{ kN sec}^2/\text{m}^4$, $L = 10 \text{ m}$, $R = \infty$) under a concentrated load

$P_y = 1000 \text{ kN}$ in the vertical direction eccentrically applied at its free end. In Table A.1 of the Appendix the geometric constants of the cross section are presented.

In Fig. 6 a model of the beam implemented in FEMAP [54] employing FEM quadrilateral solid elements is shown. In the same figure the total deflection is also recorded. It is worth here noting that in order to obtain the distributions of the kinematical components and stress resultants from the solid model, rigid diaphragms were placed in regular distances (20 in total), permitting the measurement of rotation angles and translations of the reference nodes. The existence of diaphragms also ensured the absence of local distortional phenomena of the cross sectional profiles. Results coincide with the beam formulation of the present study.

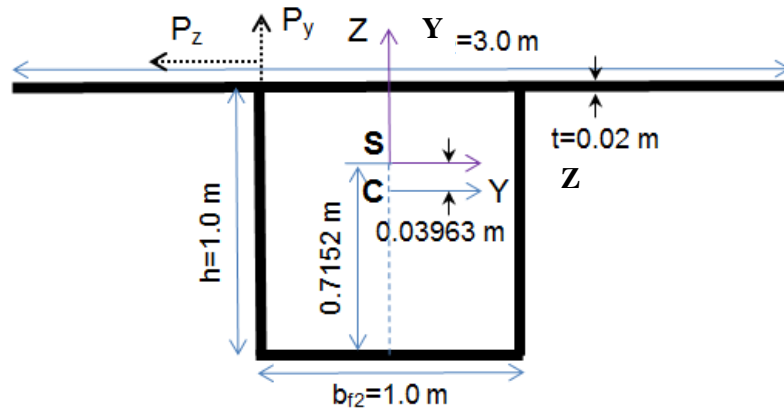


Figure 5. Box-shaped cross section of the beam of example 4.1.

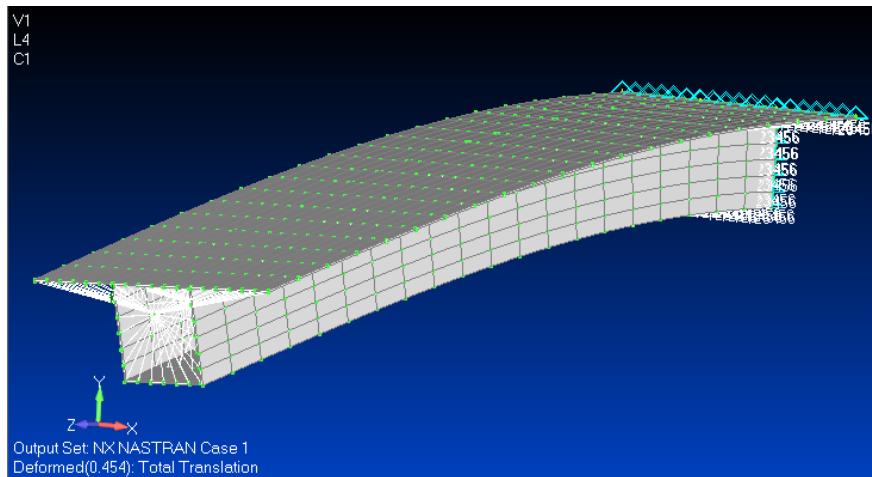


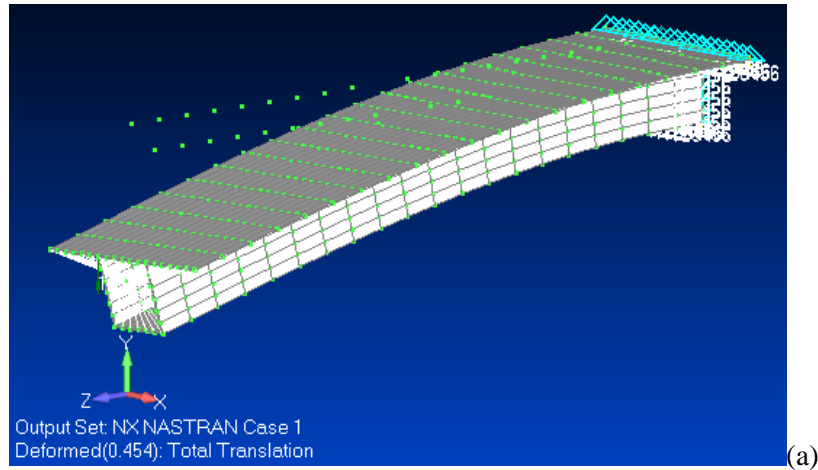
Figure 6. Model in FEMAP employing 780 quadrilateral solid finite elements. Deflection $w(x)$ is displayed along the length of the beam.

The Guide Specifications for Horizontally Curved Highway Bridges by the AASHTO [55] specify the maximum spacing of the intermediate diaphragms

$$L_D \text{ as } L_D \leq L \left(\frac{R}{200L - 7500} \right)^{1/2} \leq 25 \text{ ft} \text{ where } L \text{ and } R \text{ denote the span length}$$

and radius of curvature in feet, respectively. This provision meets the requirement that the distortional warping normal stress is limited within 10% of the bending normal stress and the transverse bending normal stress is limited to 137.3MPa or lower. In addition to this, the Hanshin Expressway Public Corporation of Japan provided the Guidelines for the Design of Horizontally Curved Girder Bridges [56], specifying the maximum spacing of the intermediate diaphragms in curved box girder with respect to that in straight box girders multiplied by a reduction factor, which is equal to unity for a span length less than 60 m. It should be noted here that the boundary conditions and the cross section shape are not taken into account for both specifications directly.

According to these guidelines, Fig. 7(a) shows the deformed shape and total translation of the beam displayed in Fig. 6 employing 2 diaphragms (one at midspan and one at the free edge) while Fig. 7(b) is the same but without the employment of any diaphragms. Results of models displayed in Figs. 6 and 7(a), which are similar to each other, almost coincide with the results obtained by the proposed beam formulation. However, it is obvious from Fig. 7(b) that the absence of diaphragms leads to a larger total translation by 18% due to the development of distortional warping. Thus, the proposed beam formulation can predict a highly accurate behavior of the 3d model in terms of simplicity and safety and comply with the guidelines without considering any distortional effects.



(a)

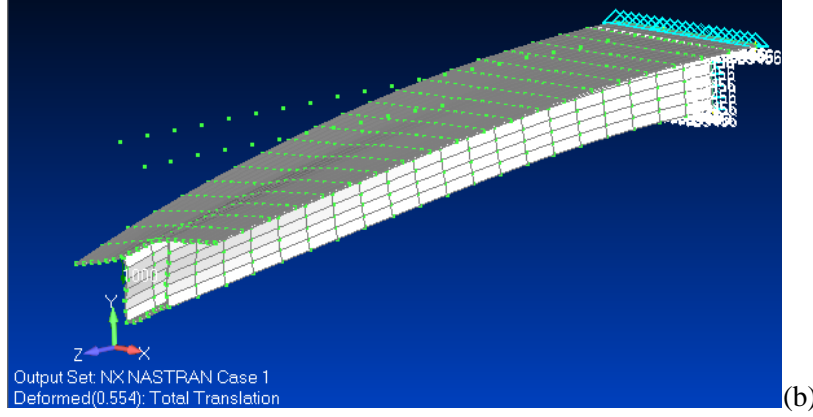


Figure 7. Deformed shapes and total vertical translation of the beam of example 4.1 (a) for 2 diaphragms and (b) without diaphragms.

Then, the same beam is considered curved having the same length and a radius of curvature $R = 6.366\text{ m}$ forming an arc of 90° angle in top view. In Fig. 8 two models of the beam implemented in FEMAP [54] employing FEM quadrilateral solid elements are shown. The difference between the two models is in the use of diaphragms in the cross section plane. In the first one 13 diaphragms have been employed while in the second model only one. The bridge beams are subjected to a vertical concentrated load $P_y = 1000\text{ kN}$ applied at the centroid of their free end cross sections. In the same figure the total deflections are also recorded. It is worth here noting that the placement of the rigid diaphragms along the length of the curved beam becomes quite cumbersome due to the complexity of the solid model. In addition to this, much more quadrilateral solid elements have been employed comparing to the straight beam formulation (Fig. 6) for accuracy reasons. Comparing the deformed shapes of the beams, it is obvious that the existence of diaphragms ensures indeed the absence of local distortional phenomena of the cross sectional profiles along the arc length while the total maximum translation is reduced by 46%. Due to the very thin-walled structure of the cross section, a plate model in FEMAP [54] has also been employed for comparison reasons with the solid model and in order to detect any possible locking phenomena present.

In Table 1 the values of the kinematical components $v(x)$, $\theta_x(x)$ and $\theta_z(x)$ for the vertical force P_y concentrically applied at the free edge of the beam are presented for i) proposed curved beam elements with NURBS (cubic), ii) a- 1500 quadrilateral plate elements with 13 diaphragms (FEMplate 13 Diaph.), ii) b- 1500 quadrilateral plate elements with 1 diaphragm (FEMplate 1 Diaph.), ii) c- 1500 quadrilateral plate elements with 2 diaphragms (FEMplate 2 Diaph.)

according to guidelines previously mentioned, iii) 10976 quadrilateral solid elements with 13 diaphragms in FEMAP 2008 (FEMsolid 13 Diaph.), iv) 10976 quadrilateral solid elements with 2 diaphragms in FEMAP 2008 (FEMsolid 2 Diaph.) according to guidelines previously mentioned and v) 10976 quadrilateral solid elements with one diaphragm in FEMAP 2008 (FEMsolid 1 Diaph.). Analysis with cubic NURBS gives results closer to the solid model with diaphragms as it is expected. The results obtained by the analysis of the solid model with diaphragms almost agree with those obtained by the plate model with diaphragms (discrepancies around 1%). However, it is important to notice that the results obtained by the respective models with only 1 diaphragm differ from each other (discrepancies vary from 15 to 23%). The solid model seems to be stiffer than the plate one while the different displacement values are exclusively related to distortional phenomena (mainly attributed to torsion) since the corresponding models with diaphragms (no distortion) show the same level of accuracy.

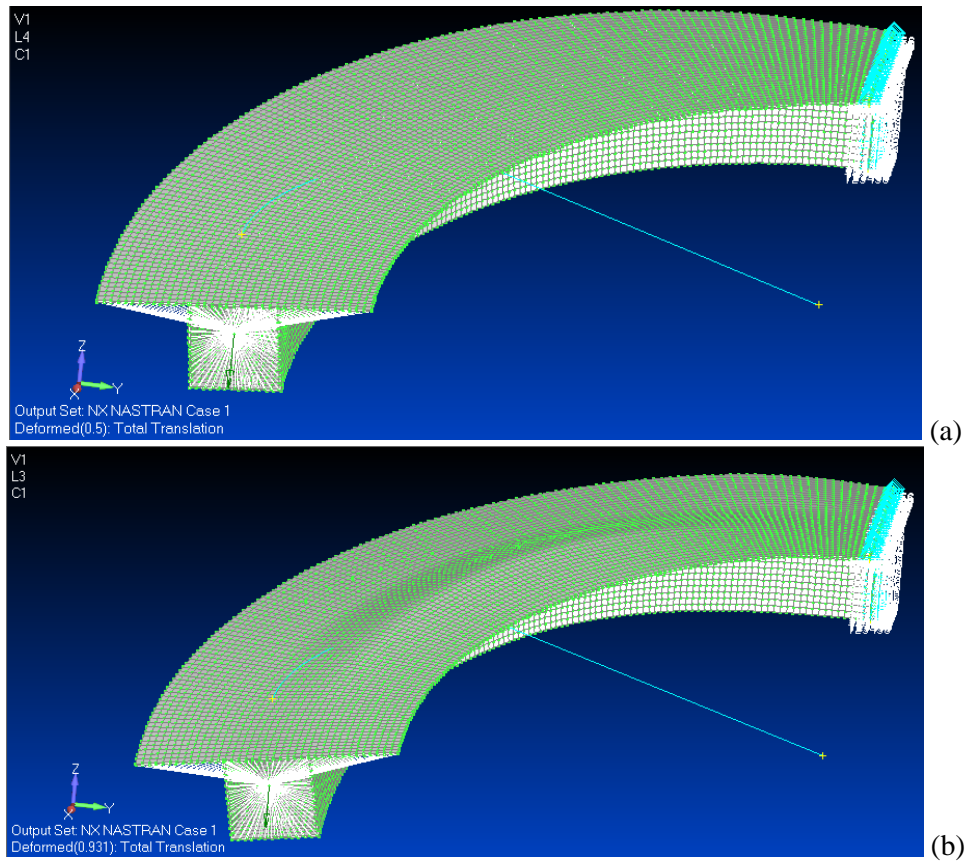
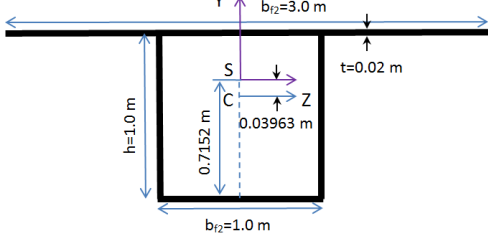



Figure 8. Deformed shapes of models in FEMAP employing 10976 quadrilateral solid finite elements and (a) 13 diaphragms or (b) one diaphragm.

Table 1. Kinematical components of the beam of Figure 5 for vertical load

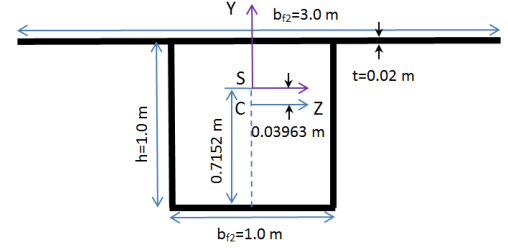

		$v(m)$ at $x=L$	$\theta_x(rad)$ at $x=L$	$\theta_z(rad)$ at $x=L$
 P_y Lateral Loading	4 cubic NURBS	0.4879	-0.0202	-0.0742
	FEMplate 13 Diaph.	0.4701	-0.0231	-0.0691
	FEMplate 2 Diaph.	0.5516	- 0.02902	-0.0812
	FEMplate 1 Diaph.	0.9748	-0.0951	-0.1470
	FEMsolid 13 Diaph.	0.4647	-0.0229	-0.0685
	FEMsolid 2 Diaph.	0.5346	-0.0279	-0.0790
	FEMsolid 1 Diaph.	0.8215	-0.0726	-0.1235

It is worth here noting that if diaphragms are placed in the solid model according to the guidelines (2 diaph. case), the vertical translation is more than the proposed formulation by 8.7%. Additionally, the angle of twist is increased by 25% and the angle of rotation due to bending by 6%. Discrepancies are slightly larger comparing to the corresponding plate model. The proposed curved beam element is obviously more strict regarding the placement of diaphragms in terms of safety against distortional effects comparing to solid and plate models. This implies the use of more diaphragms comparing to the those specified by the guidelines. In addition to this, comparing stresses between different solid models, it is proved that the normal stress due to distortion is more than the specified 10% of the normal stress due to bending for the 2 diaph. model.

A parametric study considering different radii of curvature for the same beam length and cross section has been conducted and different models have been examined. In Table 2 the discrepancies between the proposed curved beam formulation and the model with the diaphragmatic arrangement according to the

guidelines have been compiled. It is evident that as the curvature of the beam ($1/R$) becomes greater, the “error” of the specified diaphragmatic model becomes larger in an exponential rate and this rate seems to be greater for torsion. In addition to these, considering the solid model with no diaphragms and comparing to the other models, it seems that distortional effects are of more importance for large curvatures and a more refined treatment should be considered. It should also be noted that the high ratios of the dimensions to thickness of the cross section’s walls is also an important factor, especially for torsion.

Table 2. Discrepancies (%) in kinematical components’ values for different radii of curvature between the proposed model and those according to guidelines

		(%) v at $x=L$	(%) θ_x at $x=L$	(%) θ_z at $x=L$
 P_y eccentric Lateral Loading	$R=\infty$	0.00	0.64	0.00
	$R=28.65m$	1.09	1.41	1.06
	$R=12.73m$	3.03	3.40	1.91
	$R=6.37m$	8.73	27.60	6.08

The numerical procedure and the dynamic response of the beam are examined in the following. Particularly, in Fig. 9 the distribution of the vertical deflection $v(x)$ for the concentrated load $P_y = 1000 \text{ kN}$ in the vertical direction eccentrically applied this time at its free end. Curved beam elements proposed can accurately give the maximum deflection of the beam model under consideration. However, the distribution along the X axis of the arc in plan can satisfactorily be described only by the NURBS approximation of the proposed beam model due to the fact that the same NURBS functions, as for the representation of the kinematical components, have been used to describe the geometry of the curved beam and no post processing computations need to be done as in FEM beam elements. The discrepancies arising between the NURBS’ model and the solid one are probably due to the number of the diaphragms used and their positions along the length, which make the solid

model stiffer than it should be. Another reason might be shear locking problem. Additionally, the dynamic problem of the aforementioned curved beam has been studied and the values of different eigenfrequencies have been compiled in Table 3 for the same analysis cases as in the previous Table 1. It is obvious that the analysis employing the proposed curved beam formulation with NURBS approximation is closer to the FEM solid model with 13 diaphragms while the eigenfrequencies of the solid model without diaphragms are quite smaller. However, the diaphragmatic model seems to be stiffer than the proposed model especially for higher eigenfrequencies. It is also worth noting that convergence is obtained with few beam elements when NURBS are employed.

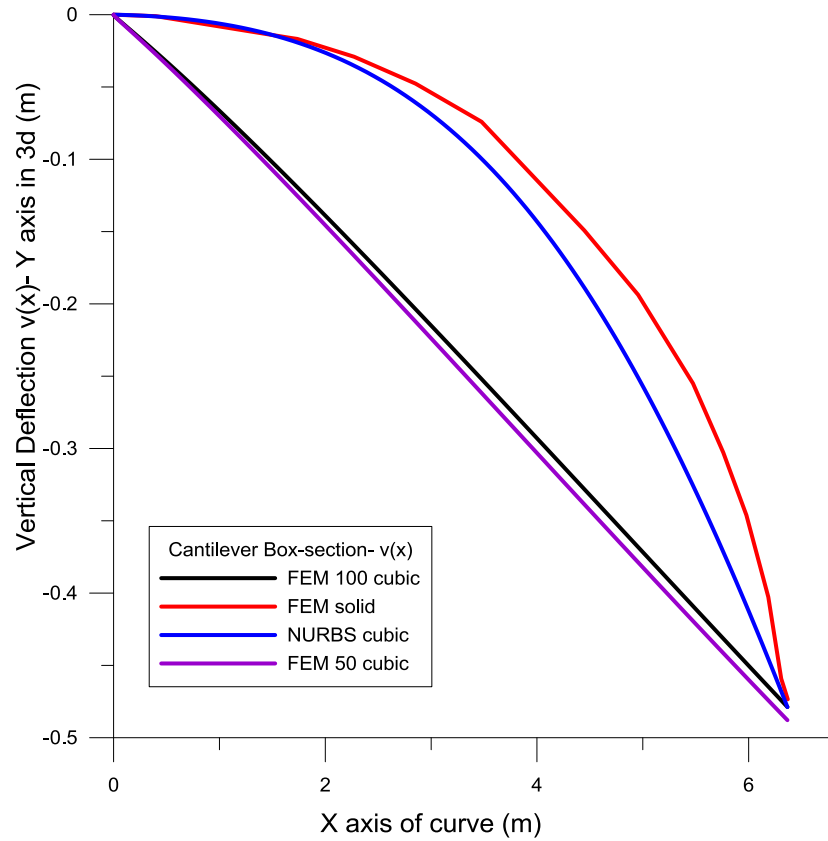


Figure 9. $v(x)$ distributions derived from the analysis of solid and curved beam models of example 4.1.

Table 3. Eigenfrequencies of the beam of Figure 5

Mode Number	FEMsolid 1 Diaph.	FEMsolid 2 Diaph.	FEMsolid 13 Diaph.	4 cubic NURBS	10cubic NURBS
1	0.1172	0.1416	0.1548	0.1317	0.1317
2	0.2556	0.2615	0.2704	0.2191	0.2191
7	0.3262	0.3644	1.0436	1.1045	1.1042
8	0.3562	0.3799	1.4233	1.2313	1.2311
9	0.4022	0.4761	1.5021	-	1.3345

In Fig. 10 the bending moment distribution is plotted for different methods employing either the proposed beam elements or the ones used in commercial software (Timoshenko beam elements). The proposed method is validated. It is worth noting here that when employing NURBS there is no need for post processing of data in order to derive stresses and stress resultants as it is the case in FEM. This is due to the fact that the same basis functions are used for the representation of geometry and kinematical components.

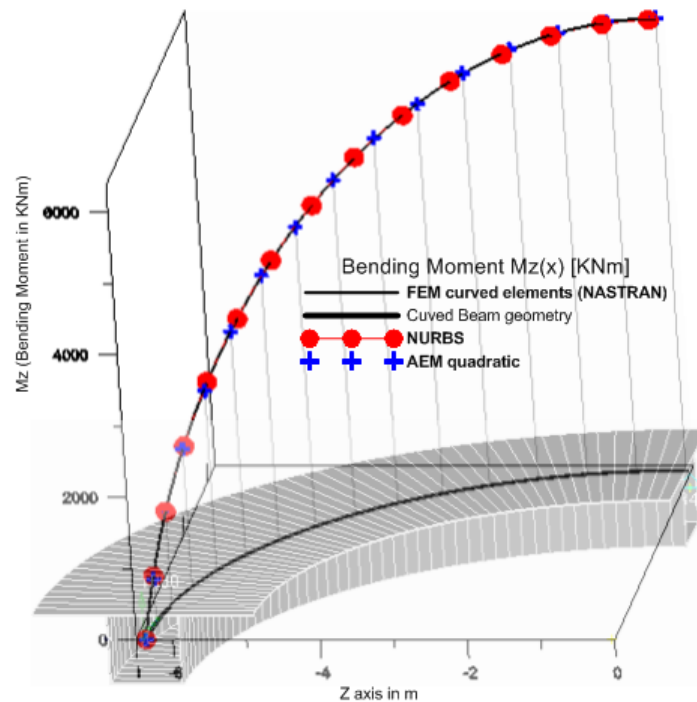


Figure 10. $M_Z(x)$ distributions derived from the analysis of curved beam models of example 4.1 and printed directly along with the curved model.

Thus, the matter is just to derive deformations and their first derivative employing the same NURBS structure for specific locations along the curve of

the beam. In addition to this, when employing AEM much more discretization elements need to be used for the same accuracy level.

In Fig. 11 the torsional moment and Bimoment distributions are plotted employing the analysis of the proposed beam model with NURBS on the curved model directly without any post-processing. Considering commercial FEM beam elements secondary Torsional Moments and Bimoments are not considered. However, the magnitude of Bimoment near the fixed support is around 10% of the total Torsional Moment and should be indeed considered in the analysis. In addition to this, secondary Torsional Moment varies from 15 (near support) to 0% of the total Torsional Moment and should also be considered.

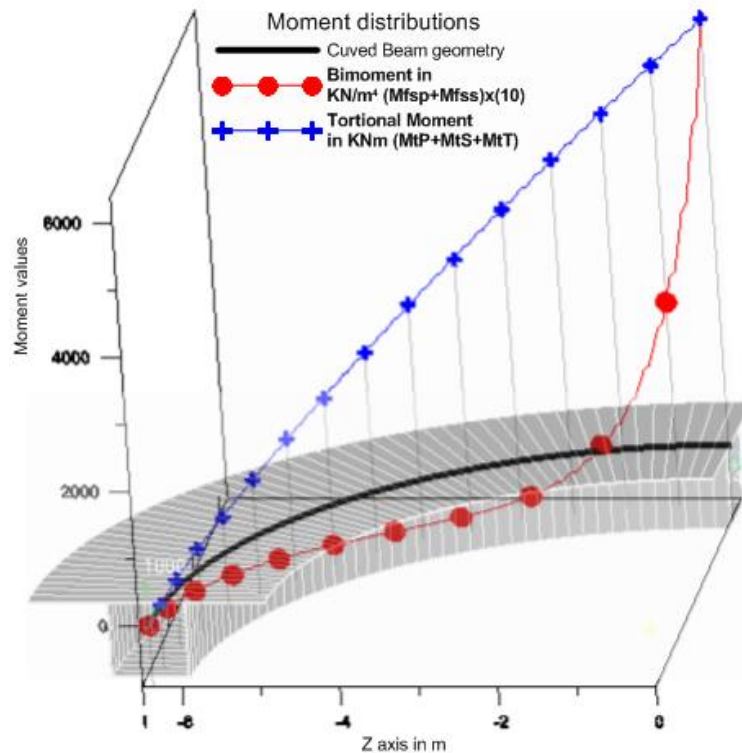


Figure 11. Torsional Moment and Bimoment distributions derived from the analysis of the proposed curved beam model of example 4.1 and printed directly along with the curved model.

Finally, in Fig. 12 the dynamic response of the curved cantilever beam previously described is plotted in terms of the tip deflection out of the curvature plane. The eigenfrequency of the first mode is 49.08 rad/sec ($T=0.0204$ seconds). A static load $P_y = 2000 \text{ kN}$ applied at the centroid of the free end has been dynamically applied in three different ways, namely suddenly applied

for 0.025 seconds, gradually applied for the first 0.005 seconds and gradually applied for 0.015 seconds. It is obvious that the amplification is less severe for the last case due to the fact that the load rise is more gradual. This is equal to 1.3 while for the case of the suddenly applied load is equal to 1.95. Regarding the other case of gradually applied load but with a shorter rise time, the amplification factor is equal to 1.83. Considering a straight beam of the same length and loading, the amplification factor for the case of transient response is equal to 1.98.

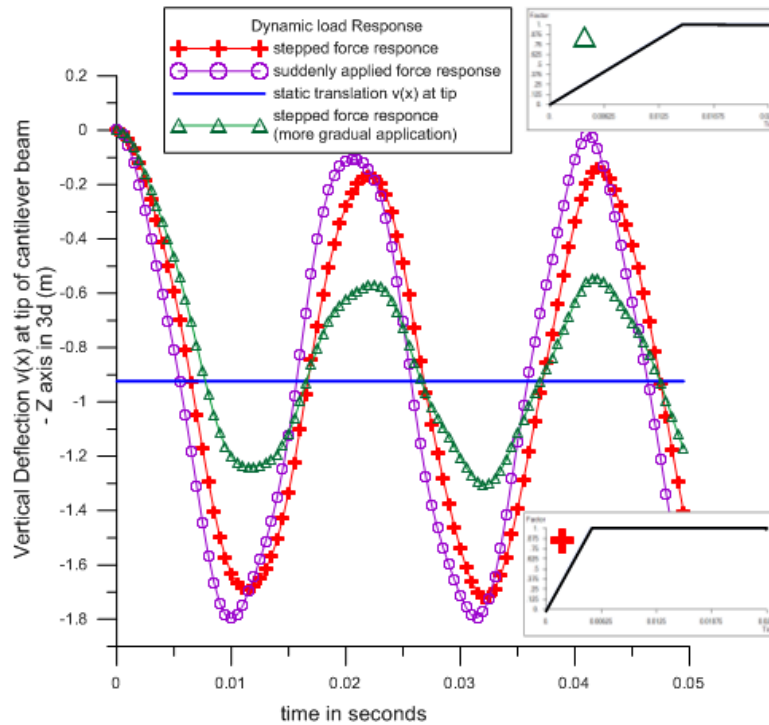


Figure 12. Deflection $v(x)$ at the tip of the curved cantilever beam shown in Fig. 8a for different cases of dynamic loading.

4.2 Moderately thin-walled monosymmetric box-shaped cross section ($t/d = 0.086, d/L = 0.086$)

A cantilever beam of a monosymmetric box-shaped (Fig. 13) cross section ($E = 3 \times 10^7 \text{ kN/m}^2$, $G = 1.5 \times 10^7 \text{ kN/m}^2$ -high strength concrete, $\rho = 2.5 \text{ t/m}^3$, $L = 40 \text{ m}$, $R = 25.465 \text{ m}$) under a concentrated load $P_y = 10000 \text{ kN}$ concentrically applied, as this is shown in Fig. 14 is examined in order to further validate the proposed beam formulation. In Table A.2 of the Appendix the geometric constants of the cross section shown in Fig. 13 are presented.

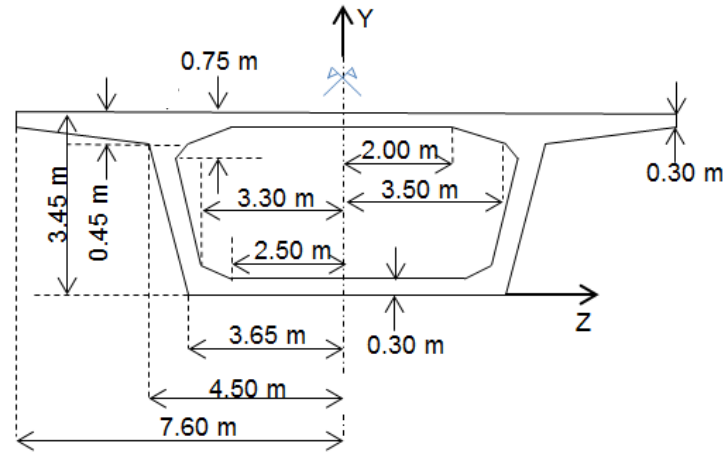


Figure 13. Box-shaped cross section of the beam of example 4.2.

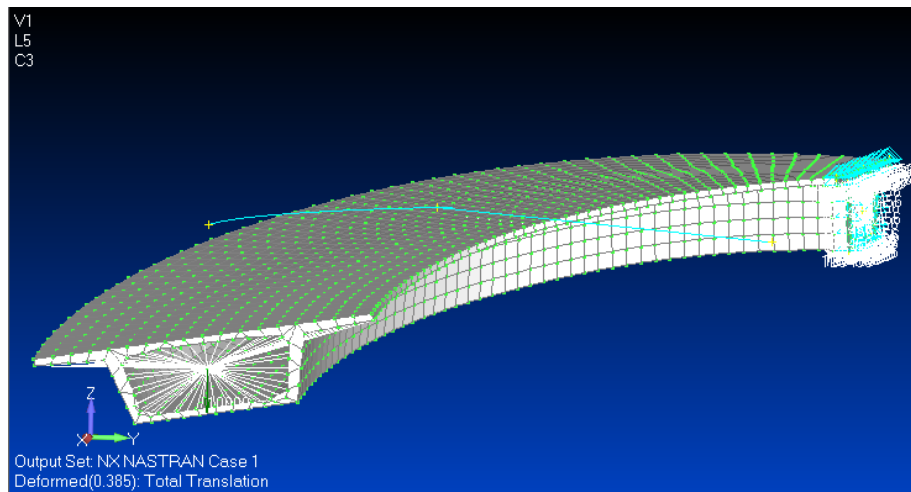
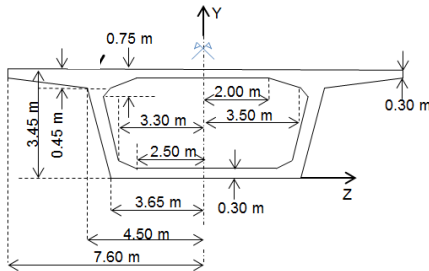


Figure 14. Deformed shape of model in FEMAP employing 2500 quadrilateral solid finite elements.

In Table 4 the values of the kinematical components $v(x)$, $\theta_x(x)$ and $\theta_z(x)$ for the vertical force P_y concentrically applied at the free edge of the beam are presented for i) proposed curved beam elements with NURBS (cubic), ii) 2500 quadrilateral solid elements in FEMAP 2008 with 1 or 2 diaphragms (FEMsolid 1 or 2 Diaph), iii) 2500 quadrilateral solid elements with 16 diaphragms according to guidelines of [55] in FEMAP [54] (FEMsolid 16 Diaph.), iv) 2500 quadrilateral solid elements with 7 diaphragms according to guidelines of [56] in FEMAP 2008 (FEMsolid 7 Diaph.) v) 2500 quadrilateral solid elements in FEMAP 2008 with 4 diaphragms (FEMsolid 4 Diaph) and vi) 40 quadratic

elements in the AEM technique (AEM 40 quad.). It is worth nothing here that when using 16 diaphragms, the vertical displacement is reduced by 23% while the angle of twist and rotation due to bending are reduced by 10% and 30%, respectively, comparing to the arrangement with 1 diaphragm. The differences in the corresponding values of the models with 2 and 4 diaphragms from those of the model with 1 diaphragm are larger in a disproportionate way when comparing the corresponding values of the same models to those of the model with 7 diaphragms. In addition to this, the proposed formulation gives results closer to the solid model with two diaphragms. Regarding the values of stresses, the discrepancies in shear stresses between models with 2, 4 and 7 diaphragms are not of much importance in comparison with those in normal stress. Additionally, the 2-diaphragmatic model exhibits stresses closer to the model with 4 diaphragms than that with 1 diaphragm. These imply that distortional effects are not of the same importance as considered in the guidelines and the use of the numbers of diaphragms specified make the solid model stiffer than it should be in real resulting in uneconomic design practices for a case like this one.

Table 4. Kinematical components of the beam of Figure 13 for vertical load

		$v(m)$ at $x=L$	$\theta_x(rad)$ at $x=L$	$\theta_z(rad)$ at $x=L$
P_y Lateral Loading	4 cubic NURBS	0.3197	-0.007029	-0.0104
	FEMsolid 1 Diaph	0.3547	-0.00867	-0.0115
	FEMsolid 2 Diaph	0.3256	-0.00782	-0.0103
	FEMsolid 7 Diaph.	0.2914	-0.00756	-0.0090
	FEMsolid 16 Diaph.	0.2746	-0.00778	-0.0081
	FEMsolid 4 Diaph.	0.3021	-0.00753	-0.0094
	AEM 40 quad.	0.3197	-0.07020	-0.0104

Similarly to previous example, in Fig. 15 the distribution of the vertical deflection $v(x)$ along the x axis of the curved geometry in plan for the concentrated load in the vertical direction mentioned previously. As it is the case in the previous example, curved beam elements proposed can accurately give the maximum deflection of the beam model under consideration. It is worth noting here that the approximation of the $v(x)$ distribution when employing quadratic elements in the AEM technique exhibits a stiffer behavior comparing to NURBS approximation.

Moreover, the dynamic case is studied and the eigenfrequencies are evaluated and compiled in Table 5 for the solid model and the proposed one analysed employing NURBS. The values of the proposed formulation are closer to the solid model with 1 or 16 diaphragms for the first five eigenfrequencies and closer to the solid one with 16 diaphragms for the last three. However, regarding the design quantities, the first eigenfrequencies are of main interest. Thus, it is implied that distortion can be prevented with few number of diaphragms.

Table 5. Eigenfrequencies of the beam of Figure 13

<i>Mode Number</i>	<i>FEMsolid 1 Diaph.</i>	<i>FEMsolid 16 Diaph.</i>	<i>cubic NURBS</i>
1	0.0488	0.0541	0.0412
2	0.1408	0.1457	0.1203
3	0.1905	0.2208	0.2501
4	0.3002	0.3885	0.3200
5	0.4643	0.5033	0.4452
6	0.5309	0.6481	0.6465
7	0.6299	0.8718	0.7046
8	0.6797	1.0252	0.9412
9	0.7125	1.1320	1.1889
10	0.7361	1.4439	1.3252

In Fig. 16 the distribution of total, primary and secondary Torsional Moments are plotted along the length of the curved beam for the concentrated load in the vertical direction. In addition to this, the Bimoment distribution has also been plotted. It is worth noting here that Torsion and Warping are of the same order of magnitude near the support for this specific cross section. Thus, Warping effect will cause important discrepancies between the commercial FEM beam elements and the one proposed in this study. Secondary Torsional Moment has a considerable value near support, too.

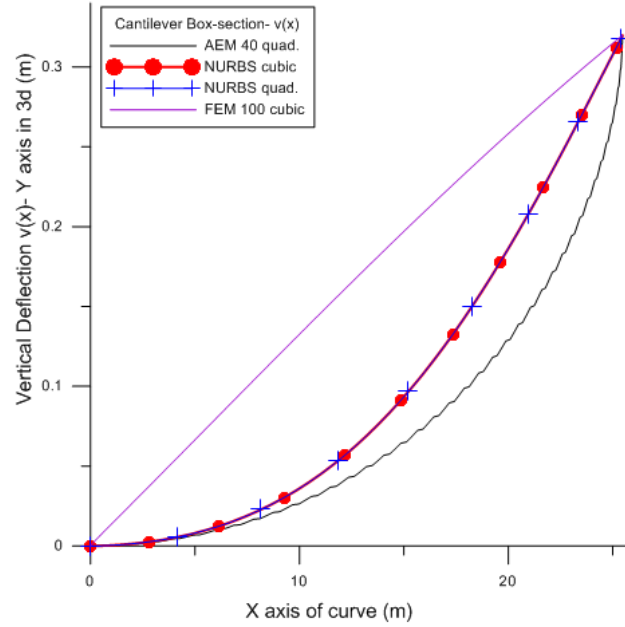


Figure 15. $v(x)$ distributions derived from the analysis of the solid and curved beam models of example 4.2.

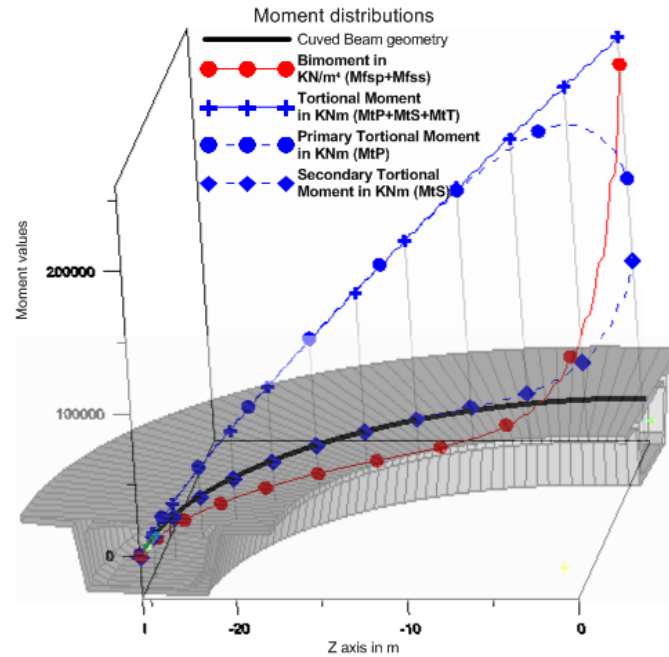


Figure 16. Torsional Moments and Bimoment distributions derived from the analysis of the proposed curved beam model of example 4.2 and printed directly along with the curved model.

Considering the curved beam of Fig. 14 with fixed end supports and a load $P_y = 20000 \text{ kN}$ applied at the centroid of the mid span, the amplification factor of the transient response for is equal to 1.90 for a system's period $T=0.127$ seconds (first mode) at time $t=0.0675$ seconds.

4.3 Concrete monosymmetric box-shaped cross section ($t/d = 0.1$, $d/L = 0.065$)

The curved beam of a concrete monosymmetric box-shaped cross section ($E = 3,25 \times 10^7 \text{ kN/m}^2$, $\nu = 0,1667$ - high strength concrete, $\rho = 2,5 \text{ t/m}^3$, $L = 33 \text{ m}$, $R = 100 \text{ m}$) shown in Fig. 17 is examined either as cantilever or clamped for static and dynamic response. In Table A.3 of the Appendix A the geometric constants of the cross section are presented.

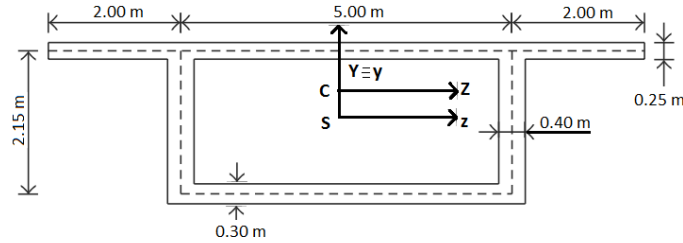


Figure 17. Box-shaped cross section of the beam of example 4.3.

According to guidelines previously mentioned for the placement of intermediate diaphragms, either 5 [55] or 6 [56] diaphragms should be at least employed in order to fulfill limitations. Considering a cantilever beam, as the less favorable case in terms of boundary conditions, under a concentrated load $P_y = 3000 \text{ kN}$ eccentrically applied at its free end, several diaphragmatic arrangements have been performed.

The distributions of the main displacements and the maximum stresses arising have been illustrated in Fig. 18. The proposed formulation with NURBS coincides with the FEM model of 6600 triangular solid elements and one rigid diaphragm created with FEMAP [54] (errors around 0% for displacements and stress resultants). The discrepancies between the proposed formulation and the solid model without any diaphragms are quite small (less than 5%) and only for the angle of twist the difference becomes larger (8.6 %). This implies that the distortion is not of much importance for this cross section and structural arrangement. Regarding the maximum normal and maximum shear stresses, it seems that the after the placement of 4 diaphragms not much difference takes place and even for less than 4 diaphragms the “errors” arising are around 5%. Thus, guidelines might lead to cost ineffective solutions for this particular curved bridge deck.

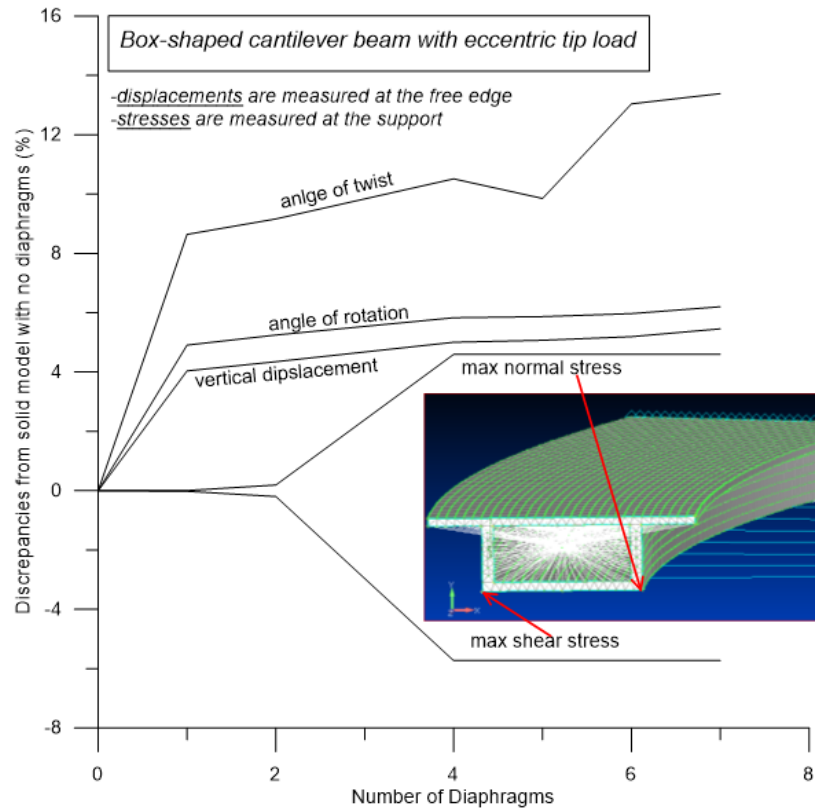


Figure 18. Discrepancies from solid model without diaphragms for a cantilever beam with the cross section shown in Fig. 17.

In addition to these, the clamped model of the same beam is considered in Fig. 19. Similarly to the previous case of the cantilever beam, the proposed formulation agrees to the solid model with one diaphragm. The discrepancies between the models become larger for displacements as the number of diaphragms increases comparing to the previous case of the cantilever beam. However, stresses, which are of more importance in this case due to the fact that the magnitude of displacements is quite low, are almost unaffected by the placement of diaphragms. Thus, it seems that boundary conditions need to be considered in the specification of diaphragms.

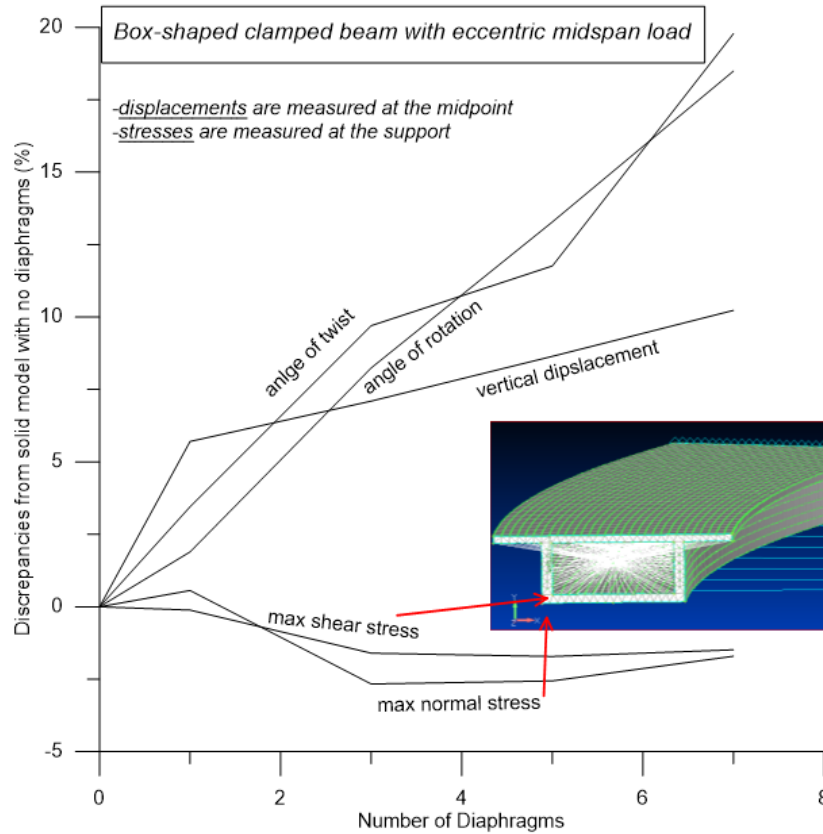


Figure 19. Discrepancies from solid model without diaphragms for a clamped beam with the cross section shown in Fig. 17.

After specifying the maximum spacing of diaphragms and employing only one, the dynamic problem of the clamped curved beam is examined. In Table 6 the eigenfrequencies are compiled for three different cases, namely proposed formulation, solid model with one diaphragm (FEMAP) and solid model without diaphragm (ANSYS-SOLID45) [57]. It is important to note that damping is considered in the last case. However, the eigenfrequencies of the proposed curved beam formulation are in general quite close to solid model without diaphragm and in fact are closer than the solid with one diaphragm, especially after the fifth mode.

Table 6. Eigenfrequencies of the clamped beam shown in Fig. 17

<i>Mode Number</i>	<i>FEMsolid 1 Diaph.</i>	<i>Solid45 no Diaph.</i>	<i>cubic NURBS</i>	<i>Description of the predominant modes</i>
1	9.72 (1.73)*	9.67 (1.22)*	9.55	First mode of vertical displacement
2	19.21 (0.65)	19.47 (0.70)	19.33	First mode of lateral bending
3	21.58 (4.62)	21.66 (4.97)	20.58	First mode of torsion
4	22.75 (1.11)	22.98 (2.10)	22.49	Second mode of vertical displacement
5	33.59 (13.74)	36.57 (4.48)	38.21	
6	37.10 (7.93)	38.67 (3.55)	40.04	
7	44.16 (3.50)	43.74 (2.57)	42.61	
8	47.68 (11.84)	51.39 (3.78)	53.33	

*) difference between the corresponding solid model and the proposed beam model (cubic NURBS)

Finally in Fig. 20 the dynamic response is obtained for the cases previously mentioned plus the solid model without diaphragm created with FEMAP [54] for comparison reasons. The models are subjected to a vertical cosine load $P_y = 100 \cos(2\pi t) \text{ kN}$ applied at midspan. It is worth noting that damping is obvious through the oscillations present at the solid model with damping (ANSYS-SOLID45) at the initial phase of its transient response. The rest of the models exhibit in general a steady state response. However, this does not affect significantly the results comparing to the other model without diaphragm (FEMAP). The placement of diaphragm causes the reduction of the vertical displacement throughout the application of the dynamic load. The proposed formulation seems to be closer to this model and exhibits a quite smooth behavior following the application of the load due to the absence of damping.

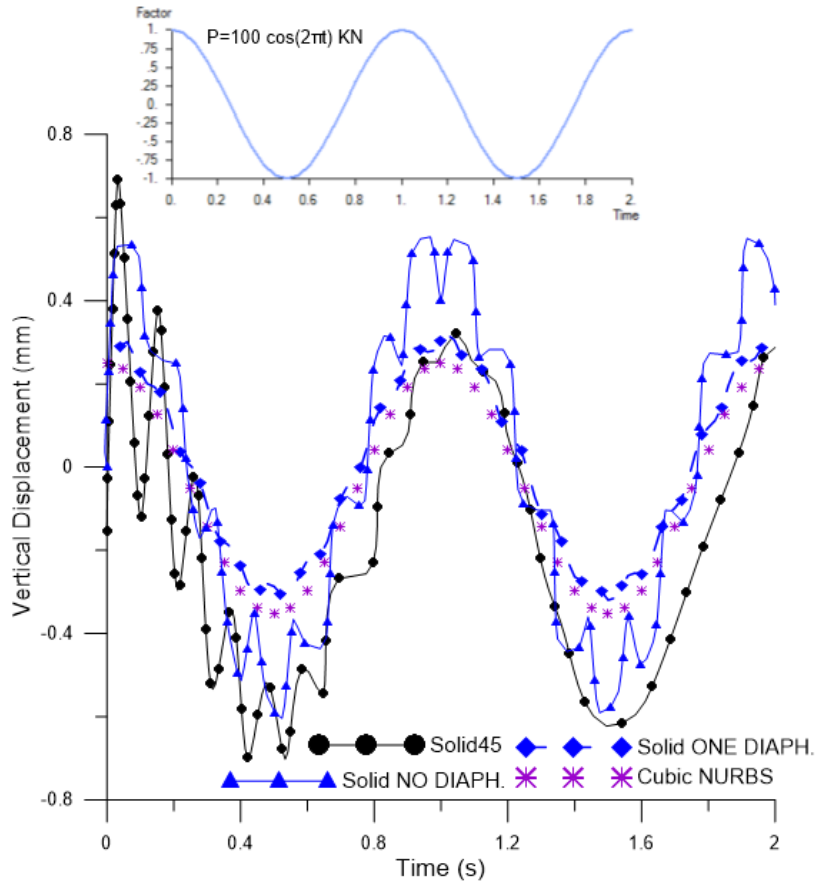


Figure 20. Box-shaped cross section of the beam of example 4.3.

5. CONCLUDING REMARKS

In this paper, the dynamic generalized warping analysis of curved beams is mainly examined. In addition to this, Isogeometric tools integrated in FEM and AEM are applied for the analysis of curved homogeneous bridge decks considering nonuniform warping effects. The presented formulation is based on advanced beam elements taking into account secondary torsional shear deformation effect and shear lag effect due to both shear and torsion. The importance of the proposed bridge beam formulation is highlighted when considering the advantages of beam models compared with solid ones, as it is mentioned in the introduction. Thus, the main purpose is for the beam formulation to remain simple and with the least number of degrees of freedom needed to describe its behavior accurately (distortional effects and local

buckling phenomena increase significantly the dimension of the problem). NURBS structures give another important advantage over solid models, especially with curved geometries, due to the fact that they do not require cumbersome pre- and post-processing while integrate curved geometry in the analysis employing the same shape functions. In addition to this, creation of coarse models with quadrilateral solid elements and diaphragms is very time-consuming. NURBS have been employed in combination with FEM or AEM beam elements and compared to FEM models employing quadrilateral or triangular solid elements and quadratic AEM beam elements. Results have also been obtained when employing diaphragms in the solid models according to guidelines of [55] and [56]. The main conclusions that can be drawn from this investigation are:

- a. Highly accurate results can in general be obtained using b-splines in the AEM technique as well as NURBS in FEM beam formulations for the static and dynamic analysis of the proposed beam element. Computational effort, including post-processing of the results, is significantly reduced by the use of NURBS comparing to FEM beam and solid models. Employment of NURBS either in FEM or in AEM results in higher convergence rates and highly accurate results with few elements. In addition to this, NURBS give more accurate values for higher frequencies comparing to traditional FEM beam elements
- b. The magnitude of Bimoment is in general not negligible comparing to the total Torsional Moment and both moments can also be of the same order of magnitude as in the example 4.2. In addition to this, secondary Torsional Moments can be significant and should also be considered in the analysis. These higher-order additional stress resultants can now be integrated in the analysis' results and plotted in alignment with the curved geometry due to the use of Isogeometric analysis.
- c. Regarding very thin-walled structures (example 4.1), guidelines for spacing of diaphragms to prevent distortional effects seem to lead to more unsafe solutions formulations when curved beams are considered due to the high level of warping and mainly the distortional one. In such cases the magnitude of the curvature is of importance. However, in stiffer structures with higher thickness to width ratios (examples 4.2 and 4.3), it seems that the guidelines applied in this study might give uneconomic solutions in order to moderate distortional effects. Thus, the specification of the maximum spacing of intermediate diaphragms should be encountered as a multi-parameter problem considering cross sectional geometry together with the plan view dimensions.
- d. Amplification factors of the dynamic response of a curved beam either for suddenly or gradually applied force are similar to those of straight beam

formulations. The use of diaphragms seems to moderate the dynamic load impact on the structure while the consideration of damping does not alters the response in a significant way.

ACKNOWLEDGEMENTS

This work has been supported by IKY Fellowships of Excellence for Postgraduate Studies in Greece-Siemens Program.

REFERENCES

- [1] Dikaros I.C., Sapountzakis E.J. Generalized Warping Analysis of Composite Beams of Arbitrary Cross Section by BEM Part I: Theoretical Considerations and Numerical Implementation. *Journal of Engineering Mechanics ASCE*, in press, DOI: 10.1061/(ASCE)EM.1943-7889.0000775.
- [2] Dikaros I.C., Sapountzakis E.J. Generalized Warping Analysis of Composite Beams of Arbitrary Cross Section by BEM Part II: Numerical Applications. *Journal of Engineering Mechanics ASCE*, in press, DOI: 10.1061/(ASCE)EM.1943-7889.0000776.
- [3] Reissner E. Analysis of shear lag in box beams by the principle of minimum potential energy. *Q. Appl. Math.* 1946; 41:268-78.
- [4] Malcolm D.J., Redwood R.G. Shear lag in stiffened box-girders. *J. Struct. Div. ASCE* 1970; 96(ST7):1403-15.
- [5] Moffatt K.R., Dowling P.J. Shear lag in steel box-girder bridges. *Struct. Engineer* 1975; 53:439-48.
- [6] Eurocode 3: Design of Steel Structures – Part 1.5: Plated Structural Elements, European Committee for Standardization, prEN 1993-1-5: 2004.
- [7] Eurocode 4: Design of Composite Steel and Concrete Structures – Part 1.1: General Rules and Rules for Buildings, European Committee for Standardization, prEN 1994-1-1: 2004.
- [8] Eurocode 4: Design of Composite Steel and Concrete Structures – Part 2: General Rules and Rules for Bridges, European Committee for Standardization, prEN 1994-2: 2004.
- [9] Ie C.A., Kosmatka J.B. On the Analysis of Prismatic Beams Using First-Order Warping Functions. *International Journal of Solids and Structures* 1992; 29(7):879-891.
- [10] Katsikadelis J.T., Sapountzakis E.J. A Realistic Estimation of the Effective Breadth of Ribbed Plates. *International Journal of Solids and Structures* 2002; 39:897-910.
- [11] Vlasov V. *Thin-walled elastic beams*. Israel Program for Scientific Translations, Jerusalem; 1963.
- [12] Sapountzakis E.J., Mokos V.G. Warping Shear Stresses in Nonuniform Torsion of Composite Bars by BEM. *Computational Methods in Applied Mechanics and Engineering* 2003; 192:4337-4353.
- [13] Mokos V.G., Sapountzakis E.J. Secondary Torsional Moment Deformation Effect by BEM. *International Journal of Mechanical Sciences* 2011; 53, 897-909.
- [14] Tsipiras V.J., Sapountzakis E.J. Secondary Torsional Moment Deformation Effect in Inelastic Nonuniform Torsion of Bars of Doubly Symmetric Cross Section by BEM. *International Journal of Non-linear Mechanics* 2012; 47, 68-84.
- [15] Murín J., Kutiš V. 3D-beam element with continuous variation of the cross-sectional area. *Comput. Struct.* 2002; 80:329-38.
- [16] Murín J. 3D beam element with changing cross sectional area. *Eng. Mech.* 1999;1:25–35 [in Slovak].
- [17] Murín J. Beam element with varying cross-section satisfying local and global equilibrium conditions. *Mech. Eng.* 1998; 49(3):208-23 [in Slovak].
- [18] El Fatmi R., Ghazouani N. Higher Order Composite Beam Theory built on Saint-Venant's

- Solution. Part-I: Theoretical Developments. *Composite Structures* 2011; 93:557-566.
- [19] Ghazouani N., El Fatmi R. Higher Order Composite Beam Theory built on Saint-Venant's Solution. Part-II: Built-in Effects Influence on the Behavior of End-Loaded Cantilever Beams. *Composite Structures* 2011; 93:567-581.
 - [20] Vlasov V. *Thin Walled Elastic Beams* 2nd Edn. National Science Foundation Washington DC; 1961.
 - [21] Dabrowski R. Warping torsion of curved box girders of non-deformable cross-section *Der Stahlbau* 1965; 34:135-141.
 - [22] Lili Zhu, Yinghua Zhao and Guangxin Wang Exact solution for in-plane displacement of redundant curved beam *Structural Engineering and Mechanics* 2010; 34(1):139-142.
 - [23] Luo Q.Z. and Li Q.S. Shear Lag of Thin-Walled Curved Box Girder Bridges *Journal of Engineering Mechanics* 2000; 126(10); 1111-1114.
 - [24] Heins C. P. and Spates K. R. Behavior of single horizontally curved girder *J. Struct. Div. ASCE* 1970; 96:1511-1524.
 - [25] Koo K. K. and Cheung Y. K. Mixed variational formulation for thin-walled beams with shear lag *Journal of Engineering Mechanics ASCE* 1989; 115:2271-2286.
 - [26] Rosen A. and Abromovich H. Galerkin method as a tool to investigate the planar and non-planar behaviour of curved beams *Comput. Struct.* 1984; 18:165-174.
 - [27] Yoo C. H. Matrix formulation of curved girders *J. Engng Mech. Div. ASCE* 1979; 105:971-987.
 - [28] Gendy A. S. and Saleeb A. F. On the finite element analysis of the Spatial response of curved beams with arbitrary thin-walled sections *Computers & Structures* 1992; 44(3):639-652.
 - [29] Dabrowski R. *Curved thin-walled girders theory and analysis*. Cement and Concrete Association; 1968.
 - [30] Park N. H., Lim N. H. and Kang Y. J. A consideration on intermediate diaphragm spacing in steel box girder bridges with a doubly symmetric section *Engineering Structures* 2003; 25:1665-1674.
 - [31] Park N. H., Choib Y. J. and Kang Y. J. Spacing of intermediate diaphragms in horizontally curved steel box girder bridges *Finite Elements in Analysis and Design* 2005; 41:925-943.
 - [32] Heins C. P. and Sahin M. A. Natural frequency of curved box girders *J Struct Div ASCE* 1979; 105(ST12):2591-600.
 - [33] Billing J.R. and Green R. Design provisions for dynamic loading of highway bridge. *Transportation Research Report 950*. Ontario Ministry of Transportation and Communications, Downsview, Ontario, Canada; 1984. p. 94-103.
 - [34] Cantieni R. Dynamic load test on highway bridges in Switzerland, 60 years experience of EMPA. Report no.211. Dubendorf, Switzerland; 1983.
 - [35] Ontario Highway Bridge Design Code (OHBDC). Ministry of Transportation and Communication, Ontario, Canada; 1983.
 - [36] Dimitrakopoulos E. G. and Zeng Q. A three-dimensional dynamic analysis scheme for the interaction between trains and curved railway bridges *Computers & Structures* 2015; 149:43-60.
 - [37] Huang X. M., Huang X. Y., Zhuo W. D., Shang-Guan P. and Li Y. Impact effect analysis for a continuous concrete curved bridge due to multi-vehicle loading *Journal of Vibration and Shock* 2012; 24:137-142.
 - [38] Shi Y., Xuan J. M. and Song Y. F. Analysis of vehicle-bridge coupling vibration of continuous girder bridge under uneven deck *Bridge Construction* 2009; 6:15-22.
 - [39] Tüfekçi E. and Doğruer O. Y. Out-of-plane free vibration of a circular arch with uniform cross-section: Exact solution *Journal of Sound and Vibration* 2006; 291:525-538.
 - [40] Huang C. S., Tseng Y. P., Chang S. H. and Hung C. L. Out-of-plane dynamic analysis of beams with arbitrarily varying curvature and cross-section by dynamic stiffness matrix method *International Journal of Solids and Structures* 2000; 37:495-513.
 - [41] Nallasivam K., Dutta A. and Talukdar S. Dynamic analysis of horizontally curved thin-

- walled box-girder bridge due to moving vehicle *Shock and Vibration* 2007; 14:229-248.
- [42] Huang D., Wang T. L. and Shahawy M. Vibration of horizontally curved box girder bridges due to vehicles *Computers and Structures* 1998; 68:513-528.
- [43] Hughes T., Cottrell J. and Bazilevs Y. *Isogeometric analysis: Toward Integration of CAD and FEA* Wiley; 2009.
- [44] Katsikadelis J.T. The Analog Equation Method. A Boundary – only Integral Equation Method for Nonlinear Static and Dynamic Problems in General Bodies *Theoretical and Applied Mechanics* 2002; 27:13-38.
- [45] Sapountzakis E.J. and Tsiptsis I.N. Generalized warping analysis of curved beams by BEM *Engineering Structures* 2015; 100:535-549.
- [46] Sapountzakis E. J. and Tsiptsis I. N. Quadratic B-splines in the analog equation method for the nonuniform torsional problem of bars *Acta Mechanica* 2014; 225:3511-3534.
- [47] Sapountzakis E. J. and Tsiptsis I. N. B-Splines in the Analog Equation Method for the Generalized Beam Analysis Including Warping Effects *Computers and Structures* 2016; in print.
- [48] Sanders J. L. Nonlinear Theories of Thin Shells *Quarterly Applied Mathematics* 1963; 21:21-36.
- [49] Timoshenko S. and Woinowsky-Krieger S. *Theory of plates and shells* McGraw-Hill; 1959.
- [50] Voyiadjis G. Z. and Karamanlidis D. *Advances in the Theory of Plates and Shells* Elsevier; 1990.
- [51] Piegl L. and Tiller W. *The NURBS Book* Berlin Heidelberg: Springer; 1997.
- [52] Oñate E. *Structural Analysis with the Finite Element Method. Linear Statics. Volume 1: Basis and Solids* CIMNE-Springer; 2009.
- [53] Davis P.J. and Rabinowitz P. *Methods of Numerical Integration* Academic Press New York; 1975.
- [54] FEMAP for Windows *Finite element modeling and post-processing software*. Help System Index Version 11.0.1; 2013.
- [55] American Association of State Highway and Transportation Officials (AASHTO). *Guide Specifications for Horizontally Curved Highway Bridges*. Washington DC; 1993.
- [56] Hanshin Expressway Public Corporation. *Guidelines for the Design of Horizontally Curved Girder Bridges*. Japan; 1988.
- [57] Yinhui Wang, Yidong Xu, Zheng Luo Haijun Wu and Liang liang Yan Spatial Finite Element Analysis for Dynamic Response of Curved Thin-Walled Box Girder Bridges *Mathematical Problems in Engineering* 2016; Volume 2016, Article ID 8460130.

APPENDIX

Table A.1. Geometric constants of the beam in Figure 5

$A = 1.1960E - 01 m^2$	$I_{\phi_S^S \phi_S^S} = 7.7889E - 05 m^6$
$I_{YY} = 5.6570E - 02 m^4$	$I_{\phi_{CZ}^P \phi_S^P} = -2.8455E - 04 m^5$
$I_{ZZ} = 1.9962E - 02 m^4$	$I_{\phi_{CZ}^P \phi_S^S} = 1.5685E - 04 m^5$
$I_{\phi_{CZ}^P \phi_{CZ}^P} = 9.9893E - 04 m^4$	$A_Z^P = 6.3665E - 02 m^2$
$A_Y^S = 2.3014E - 03 m^2$	$I_t^P = 2.0184E - 02 m^4$
$I_t^S = 3.7487E - 03 m^4$	$I_t^T = 1.4397E - 04 m^4$

$D_{\phi_{CZ}^S \phi_S^S} = -9.2153E - 04 m^3$	$D_{\phi_{CY}^S \phi_S^T} = 0.00E+00m^3$
$I_{\phi_{CY}^P \phi_S^S} = 0.00E+00m^5$	$I_{\phi_{CY}^P \phi_S^P} = 0.00E+00m^5$
$I_{\phi_{CY}^P \phi_{CY}^P} = 7.0222E - 04 m^4$	$A_Y^P = 3.2130E - 02 m^2$
$D_{\phi_{CY}^S \phi_S^S} = 0.00E+00m^3$	$D_{\phi_{CZ}^S \phi_S^T} = 3.0309E - 04 m^3$
$I_{\phi_S^P \phi_S^P} = 9.2289E - 04 m^6$	$A_Z^S = 7.2076E - 03 m^2$

Table A.2. Geometric constants of the beam in Figure 13

$A = 1.1280E+01m^2$	$I_{\phi_S^S \phi_S^S} = 1.42222320E+01m^6$
$I_{YY} = 1.69887612E+02m^4$	$I_{\phi_{CZ}^P \phi_S^P} = -2.81492352E+00m^5$
$I_{ZZ} = 1.90664591E+01m^4$	$I_{\phi_{CZ}^P \phi_S^S} = 3.96237278E+00m^5$
$I_{\phi_{CZ}^P \phi_{CZ}^P} = 3.35829281E+00m^4$	$A_Z^P = 2.60795231E+00m^2$
$A_Y^S = 7.69037695E-01m^2$	$I_t^P = 4.24643347E+01m^4$
$I_t^S = 2.70455808E+01m^4$	$I_t^T = 1.21016082E+00m^4$
$D_{\phi_{CZ}^S \phi_S^S} = 2.62674568E-01m^3$	$D_{\phi_{CZ}^S \phi_S^T} = 3.63838338E-01m^3$
$I_{\phi_{CY}^P \phi_S^S} = 6.20215034E-13m^5$	$I_{\phi_{CY}^P \phi_S^P} = -1.28945357E-13m^5$
$I_{\phi_{CY}^P \phi_{CY}^P} = 1.20295288E+00m^4$	$A_Y^P = 6.75899175E+00m^2$
$D_{\phi_{CY}^S \phi_S^S} = 1.17081534E-13m^3$	$D_{\phi_{CY}^S \phi_S^T} = 2.75075432E-14m^3$
$I_{\phi_S^P \phi_S^P} = 6.27435249E+01m^6$	$A_Z^S = 2.97414035E-01m^2$

Table A.3. Geometric constants of the beam in Figure 17

$A = 5.3700\text{E}+00\text{m}^2$	$I_{\phi_S^S \phi_S^S} = 1.84556865\text{E}+00\text{m}^6$
$I_{YY} = 2.851910\text{E}+01\text{m}^4$	$I_{\phi_{CZ}^P \phi_S^P} = -6.29061071\text{E}-01\text{m}^5$
$I_{ZZ} = 4.84561718\text{E}+00\text{m}^4$	$I_{\phi_{CZ}^P \phi_S^S} = 3.17151178\text{E}-01\text{m}^5$
$I_{\phi_{CZ}^P \phi_{CZ}^P} = 3.06077446\text{E}-01\text{m}^4$	$A_Z^P = 3.27457767\text{E}+00\text{m}^2$
$A_Y^S = 1.45066966\text{E}-01\text{m}^2$	$I_t^P = 1.02573505\text{E}+01\text{m}^4$
$I_t^S = 3.95307960\text{E}+00\text{m}^4$	$I_t^T = 2.53467905\text{E}-01\text{m}^4$
$D_{\phi_{CZ}^S \phi_S^S} = -2.94263448\text{E}-01\text{m}^3$	$D_{\phi_{CZ}^S \phi_S^T} = 9.46320932\text{E}-02\text{m}^3$
$I_{\phi_{CY}^P \phi_S^S} = -1.70696790\text{E}-14\text{m}^5$	$I_{\phi_{CY}^P \phi_S^P} = -1.22749033\text{E}-14\text{m}^5$
$I_{\phi_{CY}^P \phi_{CY}^P} = 3.04551295\text{E}-01\text{m}^4$	$A_Y^P = 1.17985944\text{E}+00\text{m}^2$
$D_{\phi_{CY}^S \phi_S^S} = -1.13071027\text{E}-14\text{m}^3$	$D_{\phi_{CY}^S \phi_S^T} = 2.49995337\text{E}-15\text{m}^3$
$I_{\phi_S^P \phi_S^P} = 4.16066218\text{E}+00\text{m}^6$	$A_Z^S = 2.88756060\text{E}-01\text{m}^2$